

Stable dynamics of micro-machined inductive contactless suspensions

Kirill Poletkin^{a,*}, Zhiqiu Lu^b, Ulrike Wallrabe^b, Jan Korvink^a, Vlad Badilita^{a,*}

^a*Institute of Microstructure Technology, Karlsruhe Institute of Technology, Germany*

^b*Department of Microsystems Engineering-IMTEK, University of Freiburg, Germany*

Abstract

In this article we present a qualitative approach to study the dynamics and stability of micro-machined inductive contactless suspensions (MIS). In the framework of this approach, the induced eddy current into a levitated micro-object is considered as a collection of m -eddy current circuits. Assuming small displacements and the quasi-static behavior of the levitated micro-object, a generalized model of MIS is obtained and represented as a set of six linear differential equations corresponding to six degrees of freedom in a rigid body by using the Lagrange-Maxwell formalism. The linear model allows us to investigate the general stability properties of MIS as a dynamic system, and these properties are synthesized in three major theorems. In particular we prove that the stable levitation in the MIS without damping is impossible. Based on the approach presented herewith, we give general guidelines for designing MIS. Additionally, we demonstrate the successful application of this technique to study the dynamics and stability of symmetric and axially symmetric MIS designs, both based on 3D micro-coil technology.

Keywords: classical mechanics, stability, dynamics, dissipative forces, positional forces, magnetic levitation, micro-systems, contactless suspension, 3D micro-coils

*Corresponding authors

Email addresses: kirill.poletkint@kit.edu (Kirill Poletkin), vlad.badilita@kit.edu (Vlad Badilita)

Nomenclature

| | |
|--------------------|---|
| \mathbf{A} | diagonal matrix of the micro-object mass and its moments of inertia |
| \mathbf{B} | diagonal matrix of damping coefficients |
| CS | contactless suspension |
| g | acceleration of gravity (m^2/s) |
| i_{cj} | j - coil current (A) |
| i_k | k -eddy current (A) |
| L-MEMS | levitating micro-electro-mechanical systems |
| L | Lagrange function (J) |
| L_{jj}^c | self inductance of j -coil (H) |
| L_{js}^c | mutual inductance between j - and s - coils ($j \neq s$) (H) |
| L_{kk}^{pm} | self inductance of k -eddy current circuit (H) |
| M_{jk} | mutual inductance between j - coils and k -eddy current circuit (H) |
| M | mass of levitating micro-object (kg) |
| MIS | micro-machined inductive contactless suspension |
| m | number of eddy current circuits |
| n | number of coils |
| F_l | generalized force (N) |
| PM | proof mass |
| \mathbf{P} | matrix of coefficients of the nonconservative positional forces |
| $\bar{\mathbf{q}}$ | vector of generalized coordinates |
| q_l | lateral linear generalized coordinate (m) |
| q_v | vertical linear generalized coordinate (m) |
| \mathbf{R} | matrix of coefficients of stiffness |
| R_{kk} | resistance of k -eddy current circuit (Ω) |
| R_{ks} | resistance of a common circuit for k - and s - eddy current circuits (Ω) |
| T_l | generalized torque (N m) |
| T | kinetic energy (J) |
| t | time (s) |
| W_m | energy stored within electromagnetic field (J) |

Greek

| | |
|-------------------------|---------------------------------------|
| α, β, θ | angular generalized coordinates (rad) |
| μ_l | damping coefficients |
| μ_0 | magnetic permeability of vacuum (H/m) |
| Π | potential energy (J) |
| Ψ | dissipation energy (J) |
| ω | frequency (rad/s) |
| j | imaginary unit $\sqrt{-1}$ |

5 *Symbols*

| | |
|-----|------------------------------------|
| * | imaginary part of complex variable |
| T | transpose operator |
| - | complex variable |

1. Introduction

Electro-magnetic levitation dramatically reduces mechanical friction between various components of micro-sensors and micro-actuators in relative movement to each other and enables significant improvements in their performance. This fact has already attracted a great interest in the MEMS research community during the past decades giving birth to a new generation of micro-devices: multi-inertial sensors with a high speed rotating rotor [1, 2], micro-gyroscopes [3, 4], micro-accelerators [5], frictionless micro-bearings [6, 7], hybrid suspensions [8],[9], bistable switches [10], linear-micro-actuators [11], and nano-force sensors [12]. It is worth noting that there is no mechanical contact or attachment between a moving (sensing) element and the housing in any of the above-mentioned micro-devices. Based on this fact, all micro-devices relying on electro-magnetic levitation can be assigned the generic name levitating-MEMS (L-MEMS).

20 A key element of L-MEMS is a contactless suspension providing the levitation and including a force field source and a micro-object (proof mass) levitated within the force field. Depending on the force field, contactless suspensions (CS) can be simply classified as electrostatic, magnetic and hybrid CS (a combination

of different principles, e.g., electrostatic, static magnetic field, variable magnetic
25 field, diamagnetic materials). The electrostatic CS has been already established
as the integrated element for L-MEMS, the fabrication process being compatible
with MEMS technologies. In contrast to the electrostatic CS in which stable
levitation is reached by active control, in a magnetic CS the levitation of the
proof mass can be achieved passively. This fact makes the latter very attractive
30 to be employed in L-MEMS, since this advantage opens additional opportunities
to improve L-MEMS performance and increase their operational capabilities by
means of hybrid CS [8, 9, 13, 14].

However, the development of magnetic CS is still lagging behind their elec-
trostatic counterparts. It is a well-known fact that magnetic levitation utilizing
35 a static magnetic field requires a diamagnetic or a superconducting (perfect
diamagnetic) proof mass. In the case of a diamagnetic proof mass, a diamag-
netic material with a susceptibility much higher than 1×10^{-4} is needed. Un-
fortunately, the strongest diamagnetic materials such as graphite and bismuth
[15] are not traditional materials for MEMS processing. In order to levitate a
40 superconducting proof mass, a cryogen-based environment is required, which
itself becomes a major limit for this application. Magnetic levitation utilizing a
time-varying magnetic field and a conducting proof mass, or magnetic levitation
based on electro-magnetic induction, does not have the disadvantages mentioned
above and becomes a very promising candidate for L-MEMS as an integrated
45 element. Recent achievements in the development of 3D micro-coils [16] and
new magnetic materials [17] have drastically reduced the heat dissipation in
MIS [18], which was the typical problem for first prototypes [3, 19–21], and
with that, the micromachining fabrication process for MIS can be considered as
fully established.

50 Advanced MIS applications require new designs of this type of suspension,
which should demonstrate improvements in MIS dynamics [22] and at the same
time provide stable levitation [23]. The latter is a key issue for designing MIS,
which has been studied since the middle of the last century, when first prototypes
of bulk inductive contactless suspensions employed in material processing (e.g.,

melting a levitated metal sphere) were demonstrated and reported in [24, 25]. Since that time, two main directions have been established in order to provide a condition of stable levitation in inductive contactless suspensions. One direction is related to directly solving the Maxwell equations. For instance, a technique based on the assumptions of a quasi-stationary electromagnetic field and perfectly conducting spheroid was developed by Ciric [26] to study axially symmetric designs. However, the given theoretical formulation in this work is so complex that another direction, which can be labelled as qualitative, was explored to avoid dealing with field equations.

In 1965, Laithwaite [27] developed a qualitative technique based on lines of constant phase, which can be used to predict the behaviour of different designs, including the condition of stable levitation. Laithwaite provided an overview of inductive suspension's designs which are currently realized in existing MIS prototypes. For instance, the MIS design employing levitation and stabilization coils, which was first demonstrated in the prototype of MIS developed by Shearwood et al. [28] in 1995, is a typical one, being used in most MIS prototypes. Earlier in 1952, using a qualitative approach, Okress et al. [25] proposed to replace a levitated sphere by an alternating magnetic dipole and have successfully studied the levitating force acting on the sphere. Recently, the same idea, together with assuming the quasi-static behavior of the levitated proof mass, was employed to develop the analytical model of MIS [29], and then this model was extended in order to analyze axially symmetric MIS designs [23]. The results were successfully applied to study the dynamics and stability of MIS based on 3D wirebonded micro-coils, as well as on planar coils [7].

The approaches mentioned above provide powerful tools for designing inductive suspensions, and in particular for designing MIS. However, in all of them the analysis of stability is reduced to the study of the minimum of potential energy for a conservative system, which is not sufficient. Indeed, in addition to potential forces, dissipative (due to air environment) and nonconservative positional forces (due to the electrical resistance in the conductive proof mass) are acting on the levitated proof mass. According to the classical theory of stability,

dissipative forces support the stable state of a system, while positional forces destroy it. Hence, it becomes necessary to determine the balance between all of these forces (potential, dissipative, and positional) to provide a comprehensive stable levitation condition in MIS. Stability becomes especially critical for MIS
90 operation in vacuum, which is extremely relevant, for instance, for micro-sensor applications.

In order to fill this gap, this article presents a generalized linear analytical model of MIS in which potential, dissipative and positional forces are taken into account. Considering the induced eddy current into a micro-object as a col-
95 lection of m -eddy current circuits, and assuming small displacements and the quasi-static behavior of the levitated micro-object (proof mass), this generalized model is represented as a set of six linear differential equations by using the Lagrange-Maxwell formalism. The number of equations in this set corresponds to the six degrees of freedom (DoF) of a rigid body. Thus, the linear model al-
100 lows us to investigate the general stability properties of an inductive contactless suspension as a dynamic system. The results of this investigation are condensed in three theorems. In particular, a theorem of unstable levitation is formulated in which we prove that the stable levitation in an inductive suspension (levitating a conductive micro-object) without damping is impossible. This theorem
105 represents the extension of the result of the classical theorem elaborated for the case of a stable potential system having equal natural frequencies subjected to nonconservative positional forces [30, page 202, Theorem 6.12]. Also, we prove that MIS subjected to only positional and dissipative forces is unstable and formulate this statement in the second theorem. Then the necessary and
110 the sufficient practical conditions are defined to provide asymptotically stable levitation in MIS based on Metelitsyn's inequality [31] and formulated in the third theorem of asymptotically stable levitation.

The presented model is the natural continuation of the qualitative approach developed in [23], the crucial difference is that here the levitated micro-object is
115 approximated by a system of magnetic dipoles instead of one single dipole. This fact increases the accuracy in the evaluation of MIS dynamical parameters (the

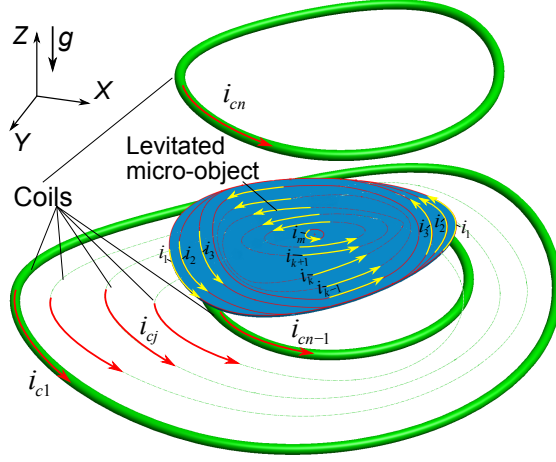


Figure 1: General schematic of micromachined contactless suspension with the m eddy current circuits: YXZ is the fixed coordinate frame; g is the gravity acceleration directed along the Z axis; i_k is the eddy current in the k -th eddy current circuit; i_{cj} is the current in the j -coil.

accuracy of modelling is dependent on the number (m) of the eddy current circuits taken into consideration), e.g., evaluating its stiffness without employing similarity coefficients, which were used in [7]. Moreover, a generalized procedure
120 for the designing of an inductive contactless suspension is proposed. Based on this procedure, the stability of a new MIS design, proposed to be used as a linear micro-transporter, is investigated. Following the procedure, the stability map is calculated as a function of design parameters. Subsequently, the experimental
125 study of the fabricated prototype of the developed linear micro-transporter helped to verify the calculated stability map. The result of this experimental study is in a good agreement with the modelling predictions.

2. Qualitative Technique

Let us consider the schematic of an inductive contactless suspension shown in Fig. 1, which consists of a system of n coils, and a levitated micro-object.
130 Each j -th coil is fed by its own alternating current denoted by i_{cj} and generates a time-variable magnetic field in space. In turn, the alternating magnetic flux

passing through the conducting micro-object induces an eddy current. The eddy current is continuously distributed within the micro-object, however this distribution is not homogeneous. This fact helps us to selectively choose the
135 m eddy current circuits having the representative behaviour of the entire eddy current distribution, as shown in Fig. 1. As seen from Fig. 1, i_k is the eddy current in the k -th eddy current circuit. The interaction between the currents in the coils and the eddy current produces the repulsive force levitating the micro-object at an equilibrium position, which can be characterized with respect
140 to the fixed coordinate frame YXZ . Considering this micro-object as a rigid body, its behaviour relative to the equilibrium position can be characterized in general by six generalized coordinates corresponding to three linear and three angular displacements, which can be denoted by q_l , $l = 1...6$. Let us define that coordinates, q_l , with indexes $l = 1, 2, 3$ are the generalized linear coordinates, while indexes $l = 4, 5, 6$ correspond to the generalized angular coordinates.
145

Adapting the generalized coordinates and the assumptions introduced above, the MIS model can be written by using the Lagrange - Maxwell equations as follows

$$\begin{cases} \frac{d}{dt} \left(\frac{\partial L}{\partial \dot{i}_k} \right) + \frac{\partial \Psi}{\partial i_k} = 0; \quad k = 1, \dots, m; \\ \frac{d}{dt} \left(\frac{\partial L}{\partial \dot{q}_l} \right) - \frac{\partial L}{\partial q_l} + \frac{\partial \Psi}{\partial \dot{q}_l} = F_l; \quad l = 1, 2, 3; \\ \frac{d}{dt} \left(\frac{\partial L}{\partial \dot{q}_l} \right) - \frac{\partial L}{\partial q_l} + \frac{\partial \Psi}{\partial \dot{q}_l} = T_l; \quad l = 4, 5, 6, \end{cases} \quad (1)$$

where $L = T - \Pi + W_m$ is the Lagrange function for the micro-object-coil system; $T = T(q_1, \dots, q_6)$ is the kinetic energy of the system; $\Pi = \Pi(q_1, \dots, q_6)$ is the potential energy of the system; $W_m = W_m(q_1, \dots, q_6, i_{c1}, \dots, i_{cn}, i_1, \dots, i_m)$ is the energy stored in the electromagnetic field; $\Psi = \Psi(\dot{q}_1, \dots, \dot{q}_6, i_1, \dots, i_m)$ is the
150 dissipation function; F_l ($l = 1, 2, 3$) and T_r ($l = 4, 5, 6$) are the generalized forces and torques, respectively, acting on the micro-object relative to the appropriate generalized coordinates.

The kinetic energy is

$$T = \frac{1}{2} \sum_{l=1}^3 M \dot{q}_l^2 + \frac{1}{2} \sum_{l=4}^6 J_l \dot{q}_l^2, \quad (2)$$

where M is the mass of the micro-object; J_l is its moment of inertia in terms of the appropriate generalized angular coordinates.

The linear generalized coordinates, q_l , $l = 1, 2, 3$, are defined in the orthogonal coordinate frame. Hence, for the further simplification of analysis, it can be assumed that the generalized coordinate q_3 is directed along the gravity acceleration g , as shown in Fig. 1. Then, the potential energy can be defined simply as follows

$$\Pi = M g q_3. \quad (3)$$

The dissipation function is

$$\Psi = \frac{1}{2} \sum_{r=1}^6 \mu_r \dot{q}_r^2 + \frac{1}{2} \sum_{k=1}^m R_k i_k^2 \pm \sum_{k=1}^m \sum_{s=1, s \neq k}^m R_{ks} i_k i_s, \quad (4)$$

where μ_r is the damping coefficient corresponding to the appropriate generalized coordinates; R_k is the electrical resistance for the k -th eddy current circuit within the micro-object; R_{ks} is the resistance of a common circuit for k -th and s -th eddy current circuits (for example, this case is shown in Fig. 1 for eddy currents i_1 , i_2 , and i_3). For generality, it is assumed that the k -th eddy current may share a common path with the s -th eddy current. The plus-minus sign corresponds to eddy currents having the same or opposite direction on the common circuit. The energy stored within the electromagnetic field can be written as

$$W_m = \frac{1}{2} \sum_{j=1}^n \sum_{s=1}^n L_{js}^c i_{cj} i_{cs} + \frac{1}{2} \sum_{k=1}^m \sum_{s=1}^m L_{ks}^o i_k i_s + \frac{1}{2} \sum_{k=1}^m \sum_{j=1}^n M_{kj} i_k i_{cj}, \quad (5)$$

155 where L_{jj}^c is the self inductance of the j -coil; L_{js}^c , $j \neq s$ is the mutual inductance between j - and s -coils; $L_{kk}^o = L_{kk}^o(q_1, \dots, q_6)$ is the self inductance of the k -eddy current circuit; $L_{ks}^o = L_{ks}^o(q_1, \dots, q_6)$, $k \neq s$ is the mutual inductance between k - and s -eddy current circuits; $M_{kj} = M_{kj}(q_1, \dots, q_6)$ is the mutual inductance between the k -eddy current circuit and the j -coil.

We now show that the induced eddy currents i_k can be expressed in terms of coil currents i_{cj} under a particular condition discussed below. Assuming that for each coil, the current i_{cj} is a periodic signal with an amplitude of I_{cj} at the

same frequency ω , we can write

$$i_{cj} = I_{cj} e^{j\omega t}, \quad (6)$$

where $j = \sqrt{-1}$. Taking the derivative of the Lagrange function with respect to the eddy current i_k , we have:

$$\frac{\partial L}{\partial i_k} = \frac{\partial W_m}{\partial i_k} = \sum_{s=1}^m L_{ks}^o i_s + \sum_{j=1}^n M_{kj} i_{cj}, \quad (7)$$

or

$$\frac{\partial L}{\partial i_k} = \frac{\partial W_m}{\partial i_k} = L_{kk}^o i_k + \sum_{s=1, s \neq k}^m L_{ks}^o i_s + \sum_{j=1}^n M_{kj} i_{cj}. \quad (8)$$

Substituting (8) into (1), the first equation of set (1) becomes

$$\begin{aligned} \frac{d}{dt} \left(\frac{\partial L}{\partial i_k} \right) + \frac{\partial \Psi}{\partial i_k} &= \sum_{r=1}^6 \frac{\partial L_{kk}^o}{\partial q_r} \frac{dq_r}{dt} i_k + L_{kk}^o \frac{di_k}{dt} \\ &+ \sum_{s=1, s \neq k}^m \left(\sum_{r=1}^6 \frac{\partial L_{ks}^o}{\partial q_r} \frac{dq_r}{dt} i_s + L_{ks}^o \frac{di_s}{dt} \right) \\ &+ \sum_{j=1}^n \left(\sum_{r=1}^6 \frac{\partial M_{kj}}{\partial q_r} \frac{dq_r}{dt} i_{cj} + M_{kj} \frac{di_{cj}}{dt} \right) + R_k i_k \pm \sum_{s=1, s \neq k}^m R_{ks} i_s = 0. \end{aligned} \quad (9)$$

Accounting for (6), the k - eddy current can be represented as

$$i_k = I_k e^{j\omega t}, \quad (10)$$

where I_k is the amplitude. Hence, Eq. (9) can be rewritten in term of the current amplitudes as follows

$$\begin{aligned} &\sum_{r=1}^6 \frac{\partial L_{kk}^o}{\partial q_r} \frac{dq_r}{dt} I_k + L_{kk}^o j\omega I_k \\ &+ \sum_{s=1, s \neq k}^m \left(\sum_{r=1}^6 \frac{\partial L_{ks}^o}{\partial q_r} \frac{dq_r}{dt} I_s + L_{ks}^o j\omega I_s \right) \\ &+ \sum_{j=1}^n \left(\sum_{r=1}^6 \frac{\partial M_{kj}}{\partial q_r} \frac{dq_r}{dt} I_{cj} + M_{kj} j\omega I_{cj} \right) + R_k I_k \pm \sum_{s=1, s \neq k}^m R_{ks} I_s = 0. \end{aligned} \quad (11)$$

Equation (11) is nonlinear due to the velocities of generalized coordinates, dq_r/dt . In fact, the analysis of the existing suspension prototypes shows that the velocity dq_r/dt can be assumed to be small. Also the frequency ω is usually

larger than 1 MHz, which corresponds to $\sim 10^7$ rad/s. Hence, Eq. (11) can be rewritten [29] as follows

$$(L_{kk}^o + R_k/(j\omega)) I_k + \sum_{s=1, s \neq k}^m (L_{ks}^o \pm R_{ks}/(j\omega)) I_s = - \sum_{j=1}^n M_{kj} I_{cj}. \quad (12)$$

It is important to note that, for higher values of the generalized velocities dq_r/dt , when the quasi-static approximation does not hold, Eq. (11) must be used. In order to define the eddy currents I_k , a set of linear equations can be compiled from (12) in a matrix form as follows:

$$\begin{pmatrix} L_{11}^o + \frac{R_1}{j\omega} & L_{12}^o \pm \frac{R_{12}}{j\omega} & \dots & L_{1k}^o \pm \frac{R_{1k}}{j\omega} & \dots & L_{1m}^o \pm \frac{R_{1m}}{j\omega} \\ L_{21}^o \pm \frac{R_{21}}{j\omega} & L_{22}^o + \frac{R_2}{j\omega} & \dots & L_{2k}^o \pm \frac{R_{2k}}{j\omega} & \dots & L_{2m}^o \pm \frac{R_{2m}}{j\omega} \\ \vdots & \vdots & \ddots & \vdots & \ddots & \vdots \\ L_{k1}^o \pm \frac{R_{k1}}{j\omega} & L_{k2}^o \pm \frac{R_{k2}}{j\omega} & \dots & L_{kk}^o + \frac{R_k}{j\omega} & \dots & L_{km}^o \pm \frac{R_{km}}{j\omega} \\ \vdots & \vdots & \ddots & \vdots & \ddots & \vdots \\ L_{m1}^o \pm \frac{R_{m1}}{j\omega} & L_{m2}^o \pm \frac{R_{m2}}{j\omega} & \dots & L_{mk}^o \pm \frac{R_{mk}}{j\omega} & \dots & L_{mm}^o + \frac{R_m}{j\omega} \end{pmatrix} \begin{pmatrix} I_1 \\ I_2 \\ \vdots \\ I_k \\ \vdots \\ I_m \end{pmatrix} = \begin{pmatrix} -\sum_{j=1}^n M_{1j} I_{cj} \\ -\sum_{j=1}^n M_{2j} I_{cj} \\ \vdots \\ -\sum_{j=1}^n M_{kj} I_{cj} \\ \vdots \\ -\sum_{j=1}^n M_{mj} I_{cj} \end{pmatrix}, \quad (13)$$

where $L_{ks}^o = L_{sk}^o$. The solution of (13) for I_k can be found by using Cramer's rule and is written as follows

$$I_k = \frac{\Delta_k}{\Delta}, \quad (14)$$

where

$$\Delta = \begin{vmatrix} L_{11}^o + \frac{R_1}{j\omega} & L_{12}^o \pm \frac{R_{12}}{j\omega} & \dots & L_{1k}^o \pm \frac{R_{1k}}{j\omega} & \dots & L_{1m}^o \pm \frac{R_{1m}}{j\omega} \\ L_{21}^o \pm \frac{R_{21}}{j\omega} & L_{22}^o + \frac{R_2}{j\omega} & \dots & L_{2k}^o \pm \frac{R_{2k}}{j\omega} & \dots & L_{2m}^o \pm \frac{R_{2m}}{j\omega} \\ \vdots & \vdots & \ddots & \vdots & \ddots & \vdots \\ L_{k1}^o \pm \frac{R_{k1}}{j\omega} & L_{k2}^o \pm \frac{R_{k2}}{j\omega} & \dots & L_{kk}^o + \frac{R_k}{j\omega} & \dots & L_{km}^o \pm \frac{R_{km}}{j\omega} \\ \vdots & \vdots & \ddots & \vdots & \ddots & \vdots \\ L_{m1}^o \pm \frac{R_{m1}}{j\omega} & L_{m2}^o \pm \frac{R_{m2}}{j\omega} & \dots & L_{mk}^o \pm \frac{R_{mk}}{j\omega} & \dots & L_{mm}^o + \frac{R_m}{j\omega} \end{vmatrix}, \quad (15)$$

$$\Delta_k = \begin{vmatrix} L_{11}^o + \frac{R_1}{j\omega} & L_{12}^o \pm \frac{R_{12}}{j\omega} & \dots & -\sum_{j=1}^n M_{1j} I_{cj} & \dots & L_{1m}^o \pm \frac{R_{1m}}{j\omega} \\ L_{21}^o \pm \frac{R_{21}}{j\omega} & L_{22}^o + \frac{R_2}{j\omega} & \dots & -\sum_{j=1}^n M_{2j} I_{cj} & \dots & L_{2m}^o \pm \frac{R_{2m}}{j\omega} \\ \vdots & \vdots & \ddots & \vdots & \ddots & \vdots \\ L_{k1}^o \pm \frac{R_{k1}}{j\omega} & L_{k2}^o \pm \frac{R_{k2}}{j\omega} & \dots & -\sum_{j=1}^n M_{kj} I_{cj} & \dots & L_{km}^o \pm \frac{R_{km}}{j\omega} \\ \vdots & \vdots & \ddots & \vdots & \ddots & \vdots \\ L_{m1}^o \pm \frac{R_{m1}}{j\omega} & L_{m2}^o \pm \frac{R_{m2}}{j\omega} & \dots & -\sum_{j=1}^n M_{mj} I_{cj} & \dots & L_{mm}^o + \frac{R_m}{j\omega} \end{vmatrix}. \quad (16)$$

Rewriting determinant (16) as follows

$$\Delta_k = \begin{vmatrix} L_{11}^o + \frac{R_1}{j\omega} & L_{21}^o \pm \frac{R_{21}}{j\omega} & \dots & L_{k1}^o \pm \frac{R_{k1}}{j\omega} & \dots & L_{m1}^o \pm \frac{R_{m1}}{j\omega} \\ L_{12}^o \pm \frac{R_{12}}{j\omega} & L_{22}^o \pm \frac{R_{22}}{j\omega} & \dots & L_{k2}^o \pm \frac{R_{k2}}{j\omega} & \dots & L_{m2}^o \pm \frac{R_{m2}}{j\omega} \\ \vdots & \vdots & \ddots & \vdots & \ddots & \vdots \\ -\sum_{j=1}^n M_{1j} I_{cj} & -\sum_{j=1}^n M_{2j} I_{cj} & \dots & -\sum_{j=1}^n M_{kj} I_{cj} & \dots & -\sum_{j=1}^n M_{mj} I_{cj} \\ \vdots & \vdots & \ddots & \vdots & \ddots & \vdots \\ L_{1m}^o \pm \frac{R_{1m}}{j\omega} & L_{2m}^o \pm \frac{R_{2m}}{j\omega} & \dots & L_{km}^o \pm \frac{R_{km}}{j\omega} & \dots & L_{mm}^o \pm \frac{R_{mm}}{j\omega} \end{vmatrix}, \quad (17)$$

and accounting for the determinant properties, (16) can be represented as the sum

$$\Delta_k = - \sum_{j=1}^n \Delta_{kj} I_{cj}, \quad (18)$$

where

$$\Delta_{kj} = - \begin{vmatrix} L_{11}^o + \frac{R_1}{j\omega} & L_{21}^o \pm \frac{R_{21}}{j\omega} & \dots & L_{k1}^o \pm \frac{R_{k1}}{j\omega} & \dots & L_{m1}^o \pm \frac{R_{m1}}{j\omega} \\ L_{12}^o \pm \frac{R_{12}}{j\omega} & L_{22}^o \pm \frac{R_{22}}{j\omega} & \dots & L_{k2}^o \pm \frac{R_{k2}}{j\omega} & \dots & L_{m2}^o \pm \frac{R_{m2}}{j\omega} \\ \vdots & \vdots & \ddots & \vdots & \ddots & \vdots \\ M_{1j} & M_{2j} & \dots & M_{kj} & \dots & M_{mj} \\ \vdots & \vdots & \ddots & \vdots & \ddots & \vdots \\ L_{1m}^o \pm \frac{R_{1m}}{j\omega} & L_{2m}^o \pm \frac{R_{2m}}{j\omega} & \dots & L_{km}^o \pm \frac{R_{km}}{j\omega} & \dots & L_{mm}^o \pm \frac{R_{mm}}{j\omega} \end{vmatrix}. \quad (19)$$

Taking the later equation into account, the current corresponding to the k-th eddy current circuit can be directly written in terms of the coils currents. Hence, Eq. (14) becomes

$$I_k = \frac{- \sum_{j=1}^n \Delta_{kj} I_{cj}}{\Delta}. \quad (20)$$

Thus, instead of $m + 6$ equations, set (1) can be reduced to six equations. Hence, the behavior of the suspension is defined only by the generalized coordinates of its mechanical part. Moreover, the number of generalized coordinates of the mechanical part can be further reduced, depending on a particular design of the suspension, as will be shown below.

Accounting for Eq. (20), the energy stored within the electromagnetic field

describing by Eq. (5) can be written via current amplitudes as follows

$$W_m = \frac{1}{2} \sum_{j=1}^n \sum_{s=1}^n L_{js}^c I_{cj} I_{cs} + \frac{1}{2} \frac{1}{\Delta^2} \sum_{k=1}^m \sum_{s=1}^m \left(L_{ks}^o \sum_{j=1}^n \sum_{i=1}^n \Delta_{kj} \Delta_{si} I_{cj} I_{ci} \right) - \frac{1}{2} \frac{1}{\Delta} \sum_{k=1}^m \sum_{j=1}^n \left(M_{kj} \sum_{s=1}^n \Delta_{ks} I_{cs} I_{cj} \right). \quad (21)$$

The set becomes

$$\begin{cases} M\ddot{q}_l + \mu_l \dot{q}_l - \frac{\partial W_m}{\partial q_l} = F_l; \quad l = 1, 2; \\ M\ddot{q}_3 + \mu_3 \dot{q}_3 + mg - \frac{\partial W_m}{\partial q_3} = F_3; \\ J_l \ddot{q}_l + \mu_l \dot{q}_l - \frac{\partial W_m}{\partial q_l} = T_l; \quad l = 4, 5, 6, \end{cases} \quad (22)$$

where the derivative of W_m with respect to a generalized coordinate has the following general form

$$\begin{aligned} \frac{\partial W_m}{\partial q_r} = & \frac{1}{2} \frac{1}{\Delta^2} \sum_{k=1}^m \sum_{s=1}^m \left(\frac{\partial L_{ks}^o}{\partial q_r} \sum_{j=1}^n \sum_{i=1}^n \Delta_{kj} \Delta_{si} I_{cj} I_{ci} \right. \\ & + \sum_{k=1}^m \sum_{s=1}^m L_{ks}^o \sum_{j=1}^n \sum_{i=1}^n \left[\frac{\partial \Delta_{kj}}{\partial q_r} \Delta_{si} + \Delta_{kj} \frac{\partial \Delta_{si}}{\partial q_r} \right] I_{cj} I_{ci} \Bigg) \\ & - \frac{1}{\Delta^3} \frac{\partial \Delta}{\partial q_r} \sum_{k=1}^m \sum_{s=1}^m \left(L_{ks}^o \sum_{j=1}^n \sum_{i=1}^n \Delta_{kj} \Delta_{si} I_{cj} I_{ci} \right) \\ & - \frac{1}{2} \frac{1}{\Delta} \sum_{k=1}^m \sum_{j=1}^n \left(\frac{\partial M_{kj}}{\partial q_r} \sum_{s=1}^n \Delta_{ks} I_{cs} I_{cj} + M_{kj} \sum_{s=1}^n \frac{\partial \Delta_{ks}}{\partial q_r} I_{cs} I_{cj} \right) \\ & + \frac{1}{2} \frac{1}{\Delta^2} \frac{\partial \Delta}{\partial q_r} \sum_{k=1}^m \sum_{j=1}^n \left(M_{kj} \sum_{s=1}^n \Delta_{ks} I_{cs} I_{cj} \right); \quad r = 1, \dots, 6. \end{aligned} \quad (23)$$

165 2.1. Linearizing

The amplitudes of the eddy currents are several orders of magnitude less than the amplitudes of the coil currents. As a result, the stored energy, which is defined by the second term in Eq. (21), is negligible compared to the third

term. Hence, Eq. (23) can be simplified as follows

$$\begin{aligned} \frac{\partial W_m}{\partial q_r} = & \underbrace{-\frac{1}{2} \frac{1}{\Delta} \sum_{k=1}^m \sum_{j=1}^n \left(\frac{\partial M_{kj}}{\partial q_r} \sum_{s=1}^n \Delta_{ks} I_{cs} I_{cj} + M_{kj} \sum_{s=1}^n \frac{\partial \Delta_{ks}}{\partial q_r} I_{cs} I_{cj} \right)}_{\text{I term}} \\ & + \underbrace{\frac{1}{2} \frac{1}{\Delta^2} \frac{\partial \Delta}{\partial q_r} \sum_{k=1}^m \sum_{j=1}^n \left(M_{kj} \sum_{s=1}^n \Delta_{ks} I_{cs} I_{cj} \right)}_{\text{II term}}; \quad r = 1, \dots, 6. \end{aligned} \quad (24)$$

The analysis of (24) shows that two sources of ponderomotive forces can be identified: those due to changing the positions of the eddy currents with respect to the coils (the first term in (24)), and those due to changing the positions of the eddy currents with respect to each other within the micro-object (the second one in (24)).

For further analysis, the derivative of stored magnetic energy, W_m , with respect to the generalized coordinates, q_r , is expanded into the Taylor series. Due to the above mentioned assumption of small displacements of the micro-object relative to the equilibrium position, the following functions taken from (24) can be expanded into the Taylor series, keeping only second order terms, as follows

$$\begin{aligned} M_{kj} &= m_0^{kj} + \sum_{l=1}^6 m_l^{kj} q_l + \frac{1}{2} \sum_{r=1}^6 \sum_{l=1}^6 m_{rl}^{kj} q_r q_l; \\ L_{ks}^o &= g_0^{ks} + \sum_{l=1}^6 g_l^{ks} q_l + \frac{1}{2} \sum_{r=1}^6 \sum_{l=1}^6 g_{rl}^{ks} q_r q_l; \\ \Delta_{ks} &= \overline{\Delta}_0^{ks} + \sum_{l=1}^6 \overline{\Delta}_l^{ks} q_l + \frac{1}{2} \sum_{r=1}^6 \sum_{l=1}^6 \overline{\Delta}_{rl}^{ks} q_r q_l; \\ \Delta &= \overline{\Delta}_0 + \sum_{l=1}^6 \overline{\Delta}_l q_l + \frac{1}{2} \sum_{r=1}^6 \sum_{l=1}^6 \overline{\Delta}_{rl} q_r q_l, \end{aligned} \quad (25)$$

where the overbar denotes a complex quantity. The coefficients of determinants Δ and Δ_{ks} are complex values due to their definitions (15) and (19), respectively, and assumed to be expressed in terms of the inductances L_{ks}^o , M_{kj} and resistances R_k and R_{ks} .

Taking into account:

$$\begin{aligned}\frac{\partial M_{kj}}{\partial q_r} &= m_r^{kj} + \sum_{l=1}^6 m_{rl}^{kj} q_l; \quad \frac{\partial L_{ks}^o}{\partial q_r} = g_r^{ks} + \sum_{l=1}^6 g_{rl}^{ks} q_l; \\ \frac{\partial \Delta_{ks}}{\partial q_r} &= \bar{\Delta}_r^{ks} + \sum_{l=1}^6 \bar{\Delta}_{rl}^{ks} q_l; \quad \frac{\partial \Delta}{\partial q_r} = \bar{\Delta}_r + \sum_{l=1}^6 \bar{\Delta}_{rl} q_l,\end{aligned}\tag{26}$$

and (25), equation (24) can be linearized as follows:

$$\begin{aligned}\frac{\partial W_m}{\partial q_r} &= -\frac{1}{2} \frac{1}{\bar{\Delta}_0} \sum_{k=1}^m \sum_{j=1}^n \left(m_r^{kj} I_{cj} \sum_{s=1}^n \bar{\Delta}_0^{ks} I_{cs} + m_0^{kj} I_{cj} \sum_{s=1}^n \bar{\Delta}_r^{ks} I_{cs} \right) \\ &+ \frac{1}{2} \frac{\bar{\Delta}_r}{\bar{\Delta}_0^2} \sum_{k=1}^m \sum_{j=1}^n \left(m_0^{kj} I_{cj} \sum_{s=1}^n \bar{\Delta}_0^{ks} I_{cs} \right) \\ &- \frac{1}{2} \frac{1}{\bar{\Delta}_0} \sum_l \left[\sum_{k=1}^m \sum_{j=1}^n \left(m_{rl}^{kj} I_{cj} \sum_{s=1}^n \bar{\Delta}_0^{ks} I_{cs} + m_r^{kj} I_{cj} \sum_{s=1}^n \bar{\Delta}_l^{ks} I_{cs} \right. \right. \\ &\quad \left. \left. + m_l^{kj} I_{cj} \sum_{s=1}^n \bar{\Delta}_r^{ks} I_{cs} + m_0^{kj} I_{cj} \sum_{s=1}^n \bar{\Delta}_{rl}^{ks} I_{cs} \right) \right] \cdot q_l \\ &+ \frac{1}{2} \frac{1}{\bar{\Delta}_0^2} \sum_l \left[\bar{\Delta}_{rl} \sum_{k=1}^m \sum_{j=1}^n \left(m_0^{kj} I_{cj} \sum_{s=1}^n \bar{\Delta}_0^{ks} I_{cs} \right) \right] \cdot q_l; \quad r = 1, \dots, 6.\end{aligned}\tag{27}$$

Accounting for (27), set (22) can be rewritten as

$$\begin{cases} M\ddot{q}_l + \mu_l \dot{q}_l + \bar{c}_{l0} + \sum_r \bar{c}_{lr} q_r = F_l; \quad l = 1, 2; \\ M\ddot{q}_3 + \mu_3 \dot{q}_3 + Mg + \bar{c}_{30} + \sum_r \bar{c}_{3r} q_r = F_3; \\ J_l \ddot{q}_l + \mu_l \dot{q}_l + \bar{c}_{l0} + \sum_r \bar{c}_{lr} q_r = T_l; \quad l = 4, 5, 6, \end{cases}\tag{28}$$

where \bar{c}_{l0} and \bar{c}_{lr} ($l, r = 1, \dots, 6$) are complex coefficients, defined by (27). At the equilibrium point, the following coefficients must hold:

$$\bar{c}_{30} = -Mg; \quad \bar{c}_{l0} = 0; \quad l = 1, 2, 4, 5, 6.\tag{29}$$

Hence, the final linearized model describing dynamics of micro-machined inductive contactless suspension becomes

$$\begin{cases} M\ddot{q}_l + \mu_l \dot{q}_l + \sum_r \bar{c}_{lr} q_r = F_l; \quad l = 1, 2, 3; \\ J_l \ddot{q}_l + \mu_l \dot{q}_l + \sum_r \bar{c}_{lr} q_r = T_l; \quad l = 4, 5, 6. \end{cases}\tag{30}$$

175 Generalized linear model (30) developed here, assuming small displacements of the levitated micro-object and its quasi-static behavior, can now be applied to study the dynamics and stability of the micromachined inductive contactless suspension.

3. Stability of Micromachined Inductive Contactless Suspensions

Let us represent linear model (30) in matrix form as

$$\mathbf{A}\ddot{\bar{\mathbf{q}}} + \mathbf{B}\dot{\bar{\mathbf{q}}} + (\mathbf{R} + j\mathbf{P})\bar{\mathbf{q}} = \mathbf{f}, \quad (31)$$

180 where $\bar{\mathbf{q}} = (\bar{q}_1, \dots, \bar{q}_6)^T$ is the column-vector of generalized coordinates, which are complex variables due to (30); $\mathbf{f} = (F_1, F_2, F_3, T_4, T_5, T_6)^T$ is the column-vector of generalized forces and torques applied to the micro-object; $\mathbf{A} = \text{diag}(M, M, M, J_4, J_5, J_6)$ is the diagonal matrix of the micro-object mass and its moments of inertia; $\mathbf{B} = \text{diag}(\mu_1, \dots, \mu_6)$ is the diagonal matrix of damping coefficients; $\mathbf{R} = (\text{Re}\{\bar{c}_{lr}\})$ and $\mathbf{P} = (\text{Im}\{\bar{c}_{lr}\})$.

According to Eq. (27), the complex coefficients can be defined as

$$\begin{aligned} \bar{c}_{lr} = & -\frac{1}{2} \frac{1}{\bar{\Delta}_0} \sum_{k=1}^m \sum_{j=1}^n \left(m_{rl}^{kj} I_{cj} \sum_{s=1}^n \bar{\Delta}_0^{ks} I_{cs} + m_r^{kj} I_{cj} \sum_{s=1}^n \bar{\Delta}_l^{ks} I_{cs} \right. \\ & \left. + m_l^{kj} I_{cj} \sum_{s=1}^n \bar{\Delta}_r^{ks} I_{cs} + m_0^{kj} I_{cj} \sum_{s=1}^n \bar{\Delta}_{rl}^{ks} I_{cs} \right) + \frac{1}{2} \frac{\bar{\Delta}_{rl}}{\bar{\Delta}_0^2} \sum_{k=1}^m \sum_{j=1}^n \left(m_0^{kj} I_{cj} \sum_{s=1}^n \bar{\Delta}_0^{ks} I_{cs} \right). \end{aligned} \quad (32)$$

The physical meanings of matrices \mathbf{A} , \mathbf{B} and \mathbf{R} are obvious. Matrix \mathbf{P} presents the coefficients of the nonconservative positional forces due to the dissipation of eddy currents. Eq. (31) can be rewritten using only real values, and at the equilibrium point the linear model is equivalent to

$$\left(\begin{array}{c|c} \mathbf{A} & 0 \\ \hline 0 & \mathbf{A} \end{array} \right) \begin{pmatrix} \ddot{\mathbf{q}} \\ \ddot{\mathbf{q}}^* \end{pmatrix} + \left(\begin{array}{c|c} \mathbf{B} & 0 \\ \hline 0 & \mathbf{B} \end{array} \right) \begin{pmatrix} \dot{\mathbf{q}} \\ \dot{\mathbf{q}}^* \end{pmatrix} + \left(\begin{array}{c|c} \mathbf{R} & -\mathbf{P} \\ \hline \mathbf{P} & \mathbf{R} \end{array} \right) \begin{pmatrix} \mathbf{q} \\ \mathbf{q}^* \end{pmatrix} = 0, \quad (33)$$

where $(\mathbf{q}|\mathbf{q}^*)^T$ is the block column-vector of twelve variables; $\mathbf{q} = \Re\{\bar{q}\}$ is the real part of \bar{q} ; $\mathbf{q}^* = \Im\{\bar{q}\}$ is the imaginary part of \bar{q} , and all block matrices have

12×12 elements. It is obvious that

$$\left(\begin{array}{c|c} \mathbf{R} & -\mathbf{P} \\ \hline \mathbf{P} & \mathbf{R} \end{array} \right) = \left(\begin{array}{c|c} \mathbf{R} & 0 \\ \hline 0 & \mathbf{R} \end{array} \right) + \left(\begin{array}{c|c} 0 & -\mathbf{P} \\ \hline \mathbf{P} & 0 \end{array} \right), \quad (34)$$

and

$$\left(\begin{array}{c|c} 0 & -\mathbf{P} \\ \hline \mathbf{P} & 0 \end{array} \right) = - \left(\begin{array}{c|c} 0 & -\mathbf{P} \\ \hline \mathbf{P} & 0 \end{array} \right)^T \quad (35)$$

is a skew-symmetric matrix which corresponds to the positional nonconservative forces.

Analysis of model (31) reveals the following general issues related to stability of MIS, which are in particular formulated in terms of three theorems, proofs
190 of which are provided in Appendix A.

Theorem 1 (Unstable levitation I). *If a micromachined inductive suspension is subjected to only electromagnetic forces defined by (23) (without dissipation forces, so that $\mathbf{B} = 0$), then stable levitation in this suspension is impossible.*

This fact can be referred to the main feature of inductive contactless suspension.
195 However, if the levitating micro-object is a perfect conductor, then $\mathbf{P} = 0$. Hence, when matrix \mathbf{R} is positive definite, stable levitation without dissipative forces becomes possible. Also another obvious conclusion can be formulated in the following corollary.

Corollary 1.1. *If a micromachined inductive suspension is subjected to only
200 electromagnetic forces, and the potential part of the electromagnetic forces is absent ($\mathbf{R} = 0$), then stable levitation in the suspension is impossible.*

Even if the dissipative forces are added to such a system without potential forces, the stable levitation in MIS is still impossible, this fact can be formulated in the second theorem below.

Theorem 2 (Unstable levitation II). *If a micromachined inductive suspen-
205 sion is subjected to electromagnetic forces having only positional $\mathbf{P} \neq 0$ ($\mathbf{R} = 0$) and dissipative forces ($\mathbf{B} > 0$), then stable levitation is impossible.*

The stable levitation in MIS can be only achieved by adding the dissipative force. Upon holding the following necessary and sufficient conditions given in the theorem below, the suspension can be asymptotically stable.

Theorem 3 (Asymptotically stable levitation). *By adding dissipative forces ($\mathbf{B} > 0$) to a micromachined inductive suspension subjected to electromagnetic forces defined by (23) and having a positive definite matrix of potential forces ($\mathbf{R} > 0$), the suspension can be asymptotically stable.*

For the asymptotically stable levitation in a MIS the necessary condition is that matrix \mathbf{A} , \mathbf{B} and \mathbf{R} should be positive definite according to Metelitsyn's inequality [31, 32, page 32]. The sufficient practical condition for asymptotically stable levitation is

$$\mu_{\min} > p_{\max} \sqrt{a_{\max}/r_{\min}}, \quad (36)$$

where μ_{\min} , and r_{\min} are the respective minimum values of \mathbf{B} and \mathbf{R} ; p_{\max} and a_{\max} are the respective maximum values of \mathbf{P} and \mathbf{A} (please see Theorem 3 in Appendix A).

Operating MIS in air, inequality (36) automatically holds due to the fact that damping forces dominate in the micro-world. Note that inequality (36) should be separately verified upon using the MIS in a vacuum environment.

4. Various Designs of Inductive Contactless Suspensions

In this section, we apply the qualitative approach developed above to analyze the dynamics and stability of several symmetric and axially symmetric designs of micromachined inductive suspensions.

A variety of axially symmetric designs of inductive suspensions based on planar and 3D micro-coils are shown in Fig. 2. In particular, the MIS design shown in Fig. 2(a) was utilized in the suspension prototype reported in [33] and proposed for its potential application as a gyroscope. The designs shown in Fig. 2(b) and (c) were employed in micro-gyroscope prototypes reported in [34] and [3, 35] in which the rotation of a disk-shaped rotor was demonstrated. The

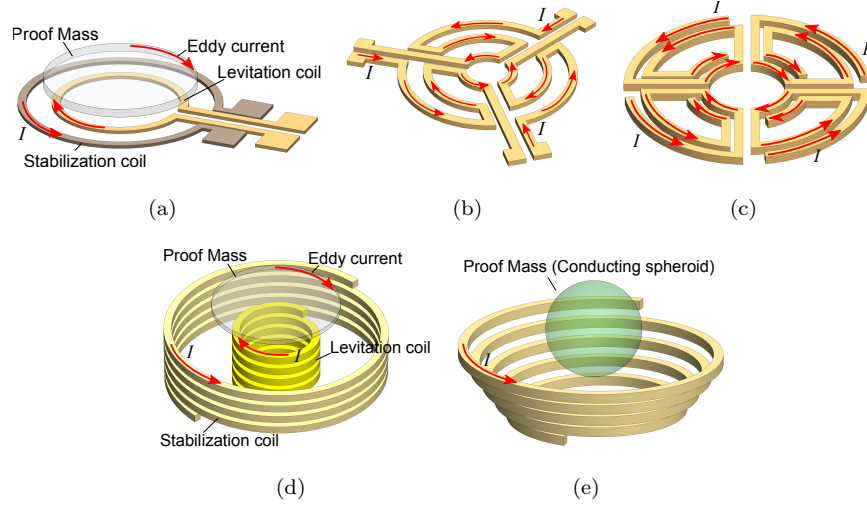


Figure 2: Axially symmetric designs based on planar and 3D micro-coils: I is the electric current.

design of a MIS based on 3D micro-coils shown in Fig. 2(d) was realized in the prototype reported in [36]. Fig. 2(e) shows the possible design of a MIS based on spiral shaped 3D micro-coils in order to levitate, for instance, a conducting micro-sphere.

235 Examples of MIS symmetric designs are shown in Fig. 3. The design shown in Fig. 3(a) was recently utilized in a prototype of accelerator for sorting micro-objects [5]. Fig. 3(b) presents the design based on 3D micro-coils, which can be employed as a linear-transporter of micro-objects. The prototype based on this design will be demonstrated below and its stability will be studied theoretically
240 and experimentally.

Due to the symmetry in the considered designs, the number of equations in set (30) can be reduced. For the case of axially symmetric designs and a spherical proof mass, the position of the levitated sphere is described by two generalized coordinates, namely q_v and q_l representing the vertical and lateral
245 linear displacements, as shown in Fig. 4(a). Let us assign the origin of the coordinate frame $X'Y'Z'$ to the equilibrium point, O , in such a way that the Z' axis is parallel to the Z axis. The coordinate frame xyz is assigned to the mass center

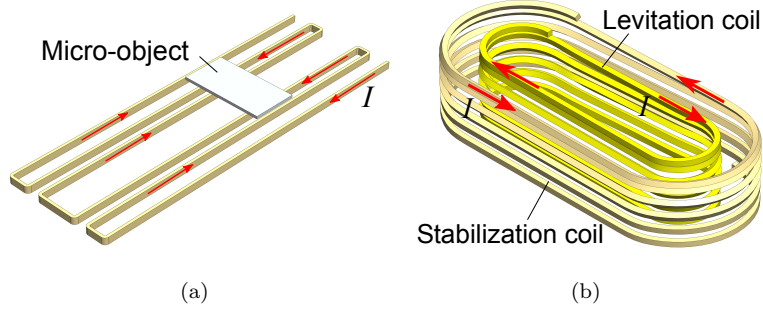


Figure 3: Symmetric designs based on planar and 3D micro-coils: I is the electric current.

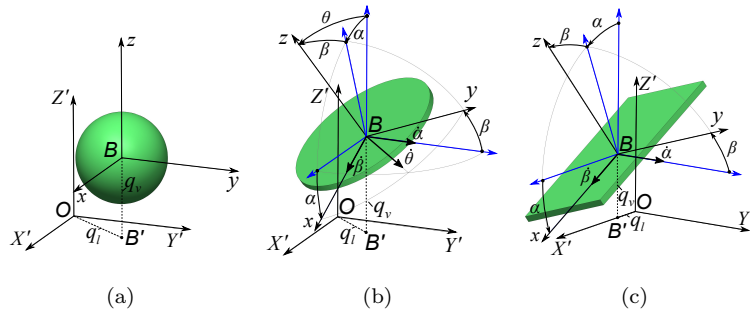






Figure 4: Coordinate frames and generalized coordinates to define the position of spherical, disk and rectangle shaped proof masses for axially symmetric and symmetric designs.

Table 1: The structures of the analytical model of the suspension as a function of design.

| Design | Levitating micro-object | Model Structure |
|-------------------|---|--|
| Axially symmetric |  | $\begin{cases} M\ddot{q}_v + \mu_v\dot{q}_v + \bar{c}_{vv}q_v = F_v; \\ M\ddot{q}_l + \mu_l\dot{q}_l + \bar{c}_{ll}q_l = F_l. \end{cases}$ |
| |  | $\begin{cases} M\ddot{q}_v + \mu_v\dot{q}_v + \bar{c}_{vv}q_v = F_v; \\ M\ddot{q}_l + \mu_l\dot{q}_l + \bar{c}_{ll}q_l + \bar{c}_{l\theta}\theta = F_l; \\ J_\theta\ddot{\theta} + \mu_\theta\dot{\theta} + \bar{c}_{\theta l}q_l + \bar{c}_{\theta\theta}\theta = T_\theta. \end{cases}$ |
| Symmetric |   | $\begin{cases} M\ddot{q}_v + \mu_v\dot{q}_v + \bar{c}_{vv}q_v = F_v; \\ M\ddot{q}_l + \mu_l\dot{q}_l + \bar{c}_{ll}q_l + \bar{c}_{l\alpha}\alpha = F_l; \\ J_\alpha\ddot{\alpha} + \mu_\alpha\dot{\alpha} + \bar{c}_{\alpha l}q_l + \bar{c}_{\alpha\alpha}\alpha = T_\alpha; \\ J_\beta\ddot{\beta} + \mu_\beta\dot{\beta} + \bar{c}_{\beta\beta}\beta = T_\beta. \end{cases}$ |

of the proof mass. Then the generalized coordinate q_v characterizes the linear displacement of sphere's centre-of-mass, parallel to the Z' axis from the $X'Y'$ surface. The generalized coordinate q_l characterizes the linear displacement of the sphere's centre-of-mass on the $X'Y'$ surface from the O point. Hence, the model is reduced to a set of two equations. The behaviour of the disk-shaped proof mass without rotation can be described by three generalized coordinates [29]. In addition to the two linear coordinates, q_l and q_v , the angular generalized coordinate, θ is used as shown in Fig. 4(b). For the symmetric designs shown in Fig. 3, it can be assumed that the levitated micro-object is in a neutral equilibrium state along the transportation line. Directing the Y' axis parallel to this line of transportation and locating the point, O , on the symmetry axis of the design, the generalized coordinates can be introduced as shown in Fig. 4(c). The generalized coordinates q_l and q_v characterize the linear displacement of the micro-object along the X' axis and the vertical one parallel to the Z' axis, respectively, while two generalized coordinates α and β characterize its angular position.

Thus, depending on the design and the shape of the levitating micro-object, the model structures describing the behaviour of the MIS, in particular the number of equations and elements of the complex matrix $\overline{\mathbf{C}}$ are already known from the defined generalized coordinates above and summarized in Table 1.

We suggest the following procedure for designing MIS. Assuming that a micromachined inductive suspension is intended for using in air, the application of our approach is reduced to the analysis of the coefficients of matrix $\mathbf{R} = (\text{Re}\{\bar{c}_{lr}\})$, whose elements are defined in (32) as functions of the design parameters. A result of this analysis would be to find the domains of these design parameters where the matrix $\mathbf{R} > 0$ is positive definite, or to demonstrate that such domains do not exist ($\mathbf{R} < 0$ is everywhere negative definite). Additionally, for a vacuum environment, it becomes necessary to define the coefficients of the matrix $\mathbf{P} = (\text{Im}\{\bar{c}_{lr}\})$, which give the required values of the damping coefficients, μ_r , in order to fulfill the condition for stable levitation as defined in Theorem 3.

4.1. Axially Symmetric Design

280 In this section, the micromachined inductive suspension design based on 3D micro-coils shown in Fig. 2(d) is analyzed. Using the theoretical model presented above, two eddy current circuits are taken into account instead of one as was done in our previous study [7]. As a result, when evaluating its dynamics and stability, an improvement in accuracy will be demonstrated, without introducing
 285 any coefficients of similarity. As it was shown in [37], the induced eddy currents are distributed along the levitated proof mass in such a way that two circuits having maximum values of eddy current density can be identified. Hence, the eddy current circuit can be represented as shown in Fig. 5(a). The eddy current circuit i_1 is the same as was given in [29] and this current flows along the edge of the proof mass. At the same time, the circuit for eddy current i_2 is defined
 290 by the levitation coil and has a circular path with radius equal to the radius of the levitation coil. Unlike the i_1 circuit, the position in space of the i_2 circuit is dependent only on the two generalized coordinates θ and q_v , and independent on the lateral displacement q_l of the proof mass, as shown in Fig. 5(b). This
 295 figure presents the case for which the lateral displacement of the proof mass takes place along the Y' axis. Due to the fact that the position of the i_1 circuit with respect to the i_2 circuit within the micro-object is variable, both sources

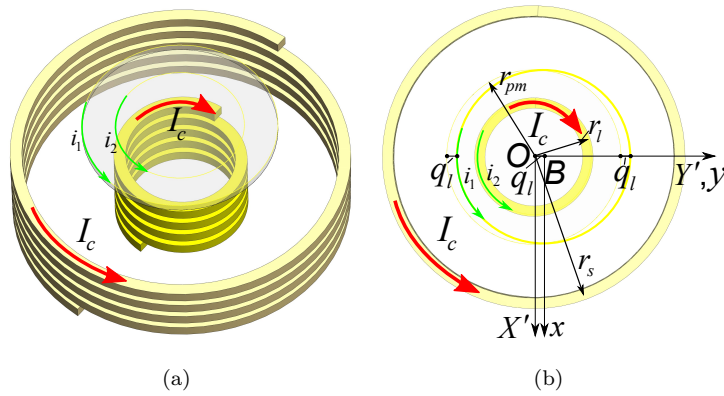


Figure 5: Schematic of 3D micromachined inductive suspension with two representative circuits for the induced eddy current.

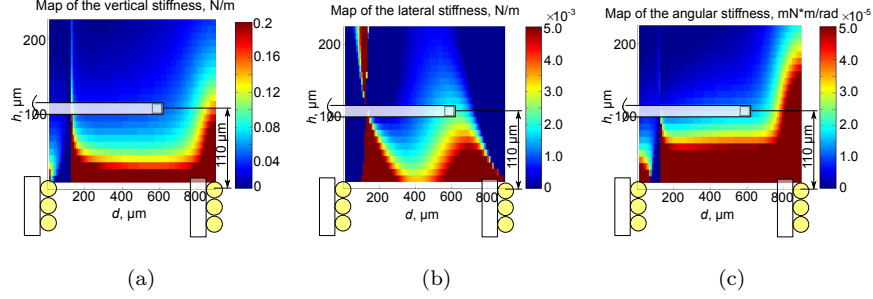


Figure 6: Maps of vertical, lateral and angular stiffness coefficients of the suspension; the square with dashed lines is the area of interest for calculation.

of ponderomotive forces defined in (24) are acting on the proof mass.

Now let us assume that the suspension is operated in air. Hence, the elements of the matrix $\mathbf{R} = (\text{Re}\{\bar{c}_{lr}\})$ will be defined as functions of the design parameters, which are the same as previously proposed in [7, 23]. Thus, $d = r_{pm} - r_l$ is the difference between the radius of the disk-shaped proof mass and the radius of the levitation coil (see, Fig. 5(b)), and h is the levitation height. In order to calculate the stiffness elements as described by (32), equations (25) are compiled as shown in Appendix B. We are using the same design of 3D MIS and the experimental parameters given in Ref. [7]: the radii of the stabilization and levitation coils are 1.9 and 1.0 mm, respectively; the pitch of coil winding is 25 μm ; the number of windings for the stabilization and levitation coils are 12 and 20, respectively; the radius of the proof mass is 1.6 mm. For an excitation current of 109 mA in both coils, the maps of the suspension stiffness coefficients

Table 2: Comparison of suspension stiffness from modelling and experiment results.

| Stiffness component | Measured values reported in [7] | Modelling reported in [7] | New model this work |
|--|---------------------------------|---------------------------|----------------------|
| Lateral, $[\text{N}\cdot\text{m}^{-1}]$ | 3.0×10^{-3} | 3.0×10^{-3} | 2.0×10^{-3} |
| Vertical, $[\text{N}\cdot\text{m}^{-1}]$ | 4.5×10^{-2} | 4.2×10^{-2} | 4.5×10^{-2} |
| Angular, $[\text{m}\cdot\text{N}\cdot\text{rad}^{-1}]$ | 1.5×10^{-8} | 0.8×10^{-8} | 1.4×10^{-8} |

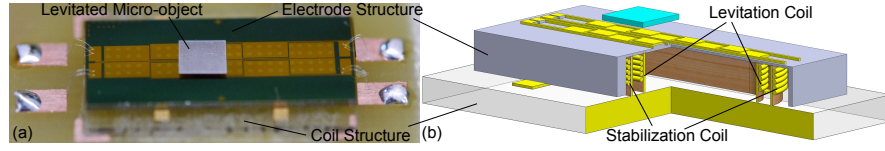


Figure 7: Micro-transporter: a) the prototype of micro-transporter glued onto a PCB under experimental testing; b) the schematic of the micro-transporter design.

coefficients are shown in Fig. 6. The results of the calculation are shown in Table 2 together with experimental and modelling results published in [7] in order to enable the direct comparison. The analysis of Table 2 shows that the developed technique allows us to evaluate the stiffness with a good enough accuracy without similarity coefficients using in [7].

4.2. Symmetric Design. Micro-linear Transporter Based on 3D Micro-coils

In this section, we analyze the symmetric design based on 3D micro-coils for its potential application as a micro-transporter, shown in Fig. 3(b). Fig. 7 shows the prototype of such a micro-transporter, together with a schematic cut-away drawing. The micro-transporter consists of two structures fabricated independently, namely the coil structure and the electrode structure, which are aligned and assembled by flip-chip bonding into one device with dimensions $20 \text{ mm} \times 7.0 \text{ mm} \times 1 \text{ mm}$ as shown in Fig. 7(a). Fig. 7(b) illustrates the interior of the micro-transporter design in a sectional view which presents the position of the 3D-coils inside the electrode structure.

The coil structure consists of two racetrack shaped solenoidal 3D wire-bonded microcoils to be used as Maglev rails, namely stabilization and levitation

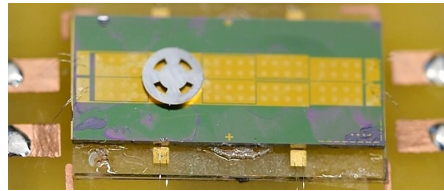


Figure 8: Successful levitation of disk shaped micro-object.

coils, fabricated on a Pyrex substrate using SU-8 2150 and UV photolithography. For electrostatic propelling of the micro-object, an array of electrodes is
 330 fabricated on a 510 μm thick silicon substrate having an oxide layer for passivation. Electrodes are patterned on top of the oxide layer by UV lithography on evaporated Cr/Au layers (20/150nm). The prototype provides stable levitation for a rectangular- as well as a disk-shaped micro-object as shown in Fig. 7(a) and Fig. 8.

335 We study the stability of the prototype operated in air environment for the case of a rectangular-shaped levitated micro-object. According to the procedure proposed above, first a representative eddy current circuit is defined. Then the equations for coefficients of Taylor series (25) are computed. The distribution of eddy currents generated by the micro-coils can be studied using a similar design of the prototype consisting of four straight wires and a rectangular shaped
 340 micro-object. Taking into account that the levitation height of the micro-object is significantly smaller than its lateral dimensions, the eddy current distribution can be represented as shown in Fig. 9. The simulation was performed for a levitation height of 100 μm and coil currents of 100 mA. The distribution in Fig. 9(a) is presented in dimensionless relative values, i.e., the ratio of the
 345 current density to its maximum value. The analysis of Fig. 9(a) shows that the representative eddy current circuit can consist of two circuits as shown in

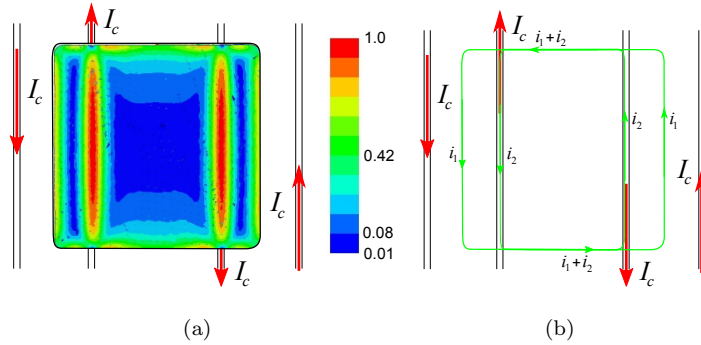


Figure 9: Eddy current induced in the rectangular micro-object: a) distribution of eddy current density; b) representative circuit.

Table 3: Parameters of the prototype of micro-transporter.

| | |
|--|--------------------|
| The levitation coil width, c_l ¹ | 1500 μm |
| The stabilization coil width, c_s ¹ | 2900 μm |
| The coils pitch of winding, p | 25 μm |
| Number of windings for stabilization coil, N | 10 |
| Number of windings for levitation coil, M | 14 |
| Length of the track, l_c | 7000 μm |
| Length of micro-object, b | 2400 μm |

Fig.9(b) covering a particular eddy current density range between 0.42 and 1.0. It is important to note that the behaviour of the eddy current circuit, i_2 , is similar to the one in the axially symmetric design and its position in space does not depend on the lateral displacement of the micro-object characterized by the generalized coordinate, q_l . Accounting for this fact, the equations to calculate the coefficients of (32) can be compiled as shown in Appendix C.

The structure of the model is given in Table 1; a condition for the stable levitation in air becomes as follows:

$$\begin{cases} c_{vv} > 0; c_{ll} > 0; c_{\alpha\alpha} > 0; c_{\beta\beta} > 0; \\ c_{ll} \cdot c_{\alpha\alpha} > c_{l\alpha}^2. \end{cases} \quad (37a)$$

$$(37b)$$

Geometrical parameters of the transporter prototype are defined by the schematic shown in Appendix C, Fig. 11(a). The parameters of this particular prototype are presented in Table 3. Considering a current of 120 mA in each coil and a phase shift of 180° , the map of stability in terms of levitation height h and width $d = (a - c_s)/2$ is shown in Fig. 10. The figure shows two cases, namely, when the length of the micro-object is $b = 2.8$ mm and $b = 0.5$ mm. In general, the analysis of the map indicates that stable levitation in this prototype is possible for a rectangular shaped micro-object with a length of 2.8 mm, when the width is within the range from 1.7 to 2.8 mm. The experimental

¹Parameter is defined in Appendix C, Fig. 11(a).

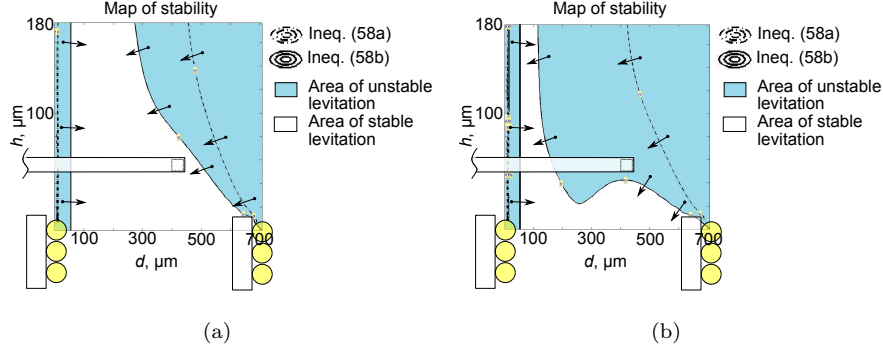


Figure 10: Map of stable levitation of the prototype 3D micro-transporter: a) the stability map for the length of the micro-object: $b = 2.8\text{mm}$; b) for the length $b = 0.5\text{mm}$.

study for the square-shaped micro-object having a size of 1.5 mm proves the fact that, for a micro-object with a width less than 1.7 mm, stable levitation is not possible. Another important feature which is reflected by this approach is that decreasing the length of a micro-object leads to a decrease in the area of stable levitation, and for a particular value of the length (in this case: $b = 0.5\text{ mm}$) stable levitation for any width is impossible. This fact was verified experimentally and agrees well with the theory as shown in Fig. 10(b).

For a micro-object with a width of 2.8 mm, the qualitative approach developed here predicted the top limit of the levitation height to be around 40 μm . The experimental study demonstrates that the levitation height can be larger than 120 μm . We see a disagreement between experimental results and the prediction of the model, however, the accuracy can be improved by adding more eddy current circuits during the calculation, as was mentioned above.

5. Discussion and conclusion

In this work we have developed the qualitative approach to study the dynamics and stability of micromachined inductive contactless suspensions, taking into account three types of forces: potential, dissipative and positional (nonconservative). The generalized linear model of MIS has been obtained based on this

approach, the analysis of which provides the general properties of the suspension as a dynamic system. In particular, Theorem 1 of unstable levitation was formulated, where we proved that the stable levitation in MIS subjected to only electromagnetic forces without dissipative forces is impossible. It is worth noting that the issue of destabilising effect of induced eddy current on a levitron was previously discussed in work in [38], but it was not mathematically formulated. Also Theorem 1 extends the classical theorem for the case of a stable potential system having equal natural frequencies subjected to nonconservative positional forces [30, page 202, Theorem 6.12].

From Theorem 3 we have an opportunity to estimate the order of magnitude of a component of positional forces having the maximum value, for instance, for 3D MIS by using the result of experimental measurements given in Table 2. In this particular case, we have $a_{max}=2.4 \times 10^{-7}$ kg, $r_{min}=1.5 \times 10^{-8}$ N m rad⁻¹ and the minimum damping coefficient corresponding to angular displacement is around $\mu_{min}=1.0 \times 10^{-8}$ N m s rad⁻¹, the maximum component of stiffness of positional forces must be less than 2.5×10^{-9} N m⁻¹ $> p_{max}$. For the one dipole approximation the component of stiffness potential and positional forces has a simple linear dependence like $\mathbf{P} = k\mathbf{R}$, where k must be less than 1×10^{-7} for 3D MIS operating in air. The interesting point is that the positional forces are even smaller. This fact was confirmed by employing the MIS in vacuum [35]. Another issue which can be pointed out here is that the stability of MIS can be adapted to a particular vacuum environment by increasing its appropriate component of stiffness.

The qualitative approach developed herewith allows us to propose the general procedure for designing MIS. In a particular case, for the symmetric MIS designs levitating rectangular- and disk-shaped micro-objects and axially symmetric designs levitating sphere and disk-shaped proof mass, the general structures of the analytical models describing their behaviour were obtained. Then, this approach was applied to study the dynamics of the prototype of axially symmetric MIS levitating the disk-shaped proof mass and the stability of the prototype of symmetric MIS levitating the rectangular-shaped proof mass, both

based on 3D micro-coil technology. In the first prototype, its stiffness components were calculated, which agree well with experimental measurements without using similarity coefficients. In the second prototype, which has been proposed for potential application as a linear transporter, its stability was studied. Theoretical analysis of its stability map as a function of width of rectangular-shaped proof mass and the levitation height, showed that the stable levitation is possible when the width of proof mass is larger than the width of the levitation coil, c_l , and less than the width of stabilization coils, c_s . In the case of equality between widths of proof mass and the stabilization coil the stable levitation is impossible. This fact agrees with the experimental study. Also theoretically we show the effect of the proof mass length on the stability. Reducing the length of the proof mass, decreases the area of stability. In particular, for a width of the proof mass of 2.8 mm, when the length of the proof mass is less than 0.5 mm, the stable levitation in the presented design is not possible. This observation was also verified experimentally.

Acknowledgment

KP acknowledges with thanks the support of the Alexander von Humboldt Foundation. JGK acknowledges support from the European Research Council (ERC) under grant no. 290586 NMCEL.

References

References

- [1] T. Murakoshi, Y. Endo, K. Fukatsu, S. Nakamura, M. Esashi, Electrostatically levitated ring-shaped rotational gyro/accelerometer, Jpn. J. Appl. Phys 42 (4B) (2003) 2468–2472.
- [2] S. Nakamura, MEMS inertial sensor toward higher accuracy & multi-axis sensing, in: Sensors, 2005 IEEE, IEEE, 2005, pp. 4–pp.

- [3] C. Shearwood, K. Ho, C. Williams, H. Gong, Development of a levitated micromotor for application as a gyroscope, *Sensor. Actuat. A-Phys.* 83 (1-3) (2000) 85–92.
- [4] Y. Su, Z. Xiao, Z. Ye, K. Takahata, Micromachined graphite rotor based on diamagnetic levitation, *Electron Device Letters, IEEE* 36 (4) (2015) 393–395.
- [5] I. Sari, M. Kraft, A MEMS linear accelerator for levitated micro-objects, *Sensor. Actuat. A-Phys.* 222 (2015) 15–23.
- [6] T. Coombs, I. Samad, D. Ruiz-Alonso, K. Tadinada, Superconducting micro-bearings, *Applied Superconductivity, IEEE Transactions on* 15 (2) (2005) 2312–2315.
- [7] Z. Lu, K. Poletkin, B. d. Hartogh, U. Wallrabe, V. Badilita, 3D micro-machined inductive contactless suspension: Testing and modeling, *Sensors and Actuators A Physical* 220 (2014) 134–143.
- [8] K. Poletkin, Z. Lu, U. Wallrabe, V. Badilita, A new hybrid micromachined contactless suspension with linear and angular positioning and adjustable dynamics, *Journal of Microelectromechanical Systems* 24 (5) (2015) 1248–1250. doi:10.1109/JMEMS.2015.2469211.
- [9] K. Poletkin, A novel hybrid contactless suspension with adjustable spring constant, in: *Solid-State Sensors, Actuators and Microsystems (TRANSDUCERS)*, 2017 Transducers-2017 19th International Conference on, IEEE, 2017, p. in press.
- [10] C. Dieppedale, B. Desloges, H. Rostaing, J. Delamare, O. Cugat, J. Meunier-Carus, Magnetic bistable micro-actuator with integrated permanent magnets, in: *Proc. IEEE Sensors*, Vol. 1, 2004, pp. 493–496.
- [11] C. Ruffert, R. Gehrking, B. Ponick, H. H. Gatzert, Magnetic levitation assisted guide for a linear micro-actuator, *Magnetics, IEEE Transactions on* 42 (11) (2006) 3785–3787.

- [12] J. Abadie, E. Piat, S. Oster, M. Boukallel, Modeling and experimentation of a passive low frequency nanoforce sensor based on diamagnetic levitation, *Sensor. Actuat. A-Phys.* 173 (1) (2012) 227–237.
- 470 [13] K. Liu, W. Zhang, W. Liu, W. Chen, K. Li, F. Cui, S. Li, An innovative micro-diamagnetic levitation system with coils applied in micro-gyroscope, *Microsystem technologies* 16 (3) (2010) 431–439.
- [14] K. V. Poletkin, A. I. Chernomorsky, C. Shearwood, A proposal for micro-machined accelerometer, base on a contactless suspension with zero spring constant, *IEEE Sensors J.* 12 (07) (2012) 2407–2413. doi:10.1109/JSEN.2012.2188831.
- 475 [15] M. Simon, L. Heflinger, A. Geim, Diamagnetically stabilized magnet levitation, *American Journal of Physics* 69 (6) (2001) 702–713.
- [16] K. Kratt, V. Badilita, T. Burger, J. Korvink, U. Wallrabe, A fully MEMS-compatible process for 3D high aspect ratio micro coils obtained with an automatic wire bonder, *Journal of Micromechanics and Microengineering* 20 (2010) 015021.
- 480 [17] S. G. Mariappan, A. Moazenzadeh, U. Wallrabe, Polymer magnetic composite core based microcoils and microtransformers for very high frequency power applications, *Micromachines* 7 (4).
- [18] K. Poletkin, A. Moazenzadeh, S. G. Mariappan, Z. Lu, U. Wallrabe, J. G. Korvink, V. Badilita, Polymer magnetic composite core boosts performance of 3D micromachined inductive contactless suspension, *IEEE Magnetics Letters* (accepted). doi:10.1109/LMAG.2016.2612181. URL <http://dx.doi.org/10.1109/LMAG.2016.2612181>
- 485 [19] R. Yates, C. Williams, C. Shearwood, P. Mellor, A micromachined rotating gyroscope, in: *Silicon Fabricated Inertial Instruments* (Digest No: 1996/227), IEE Colloquium on, IET, 1996, pp. 4/1–4/6.
- 490

- [20] N.-C. Tsai, W.-M. Huan, C.-W. Chiang, Magnetic actuator design for single-axis micro-gyroscopes, *Microsyst Technol* 15 (2009) 493 – 503.
- 495 [21] Z. Lu, K. Poletkin, U. Wallrabe, V. Badilita, Performance characterization of micromachined inductive suspensions based on 3D wirebonded micro-coils, *Micromachines* 5 (4) (2014) 1469–1484.
- [22] B. Xu, D. Chen, H. Zhang, R. Zhou, Dynamic analysis and modeling of a novel fractional-order hydro-turbine-generator unit, *Nonlinear Dynamics* 81 (3) (2015) 1263–1274.
- 500 [23] K. Poletkin, A. Chernomorsky, C. Shearwood, U. Wallrabe, A qualitative analysis of designs of micromachined electromagnetic inductive contactless suspension, *International Journal of Mechanical Sciences* 82 (2014) 110–121. doi:10.1016/j.ijmecsci.2014.03.013.
- 505 URL <http://authors.elsevier.com/sd/article/S0020740314000897>
- [24] J. Beams, J. Young, J. Moore, The production of high centrifugal fields, *Journal of Applied Physics* 17 (11) (1946) 886–890.
- [25] E. Okress, D. Wroughton, G. Comenetz, P. Brace, J. Kelly, Electromagnetic levitation of solid and molten metals, *Journal of Applied Physics* 23 (5) (1952) 545–552.
- 510 [26] I. Ciric, Electromagnetic levitation in axially symmetric systems, *Rev. Roum. Sci. Tech. Ser. Electrotech. & Energ* 15 (1) (1970) 35–73.
- [27] E. Laithwaite, Electromagnetic levitation, *Electrical Engineers, Proceedings of the Institution of* 112 (12) (1965) 2361–2375.
- 515 [28] C. Shearwood, C. Williams, P. Mellor, R. Yates, M. Gibbs, A. Mattingley, Levitation of a micromachined rotor for application in a rotating gyroscope, *Electron. Lett.* 31 (21) (1995) 1845–1846.
- [29] K. Poletkin, A. I. Chernomorsky, C. Shearwood, U. Wallrabe, An analytical model of micromachined electromagnetic inductive contactless

- suspension., in: the ASME 2013 International Mechanical Engineering Congress & Exposition, ASME, San Diego, California, USA, 2013, pp. V010T11A072–V010T11A072. doi:10.1115/IMECE2013-66010.
URL <http://proceedings.asmedigitalcollection.asme.org/proceeding.aspx?articleid=1859067>
- [30] D. R. Merkin, Introduction to the Theory of Stability, Vol. 24, Springer Science & Business Media, 2012.
- [31] I. Metelitsyn, On gyroscopic stabilization, in: Dokl. Akad. Nauk SSSR, Vol. 86, 1952, pp. 31–34.
- [32] A. P. Seyranian, A. A. Mailybaev, Multiparameter stability theory with mechanical applications, Vol. 13, World Scientific, 2003.
- [33] C. Williams, C. Shearwood, P. Mellor, A. Mattingley, M. Gibbs, R. Yates, Initial fabrication of a micro-induction gyroscope, Microelectron. Eng. 30 (1-4) (1996) 531–534.
- [34] C. Williams, C. Shearwood, P. Mellor, R. Yates, Modelling and testing of a frictionless levitated micromotor, Sensors and Actuators A: Physical 61 (1) (1997) 469–473.
- [35] W. Zhang, W. Chen, X. Zhao, X. Wu, W. Liu, X. Huang, S. Shao, The study of an electromagnetic levitating micromotor for application in a rotating gyroscope, Sensor. Actuat. A-Phys. 132 (2) (2006) 651–657.
- [36] V. Badilita, M. Pauls, K. Kratt, U. Wallrabe, Contactless magnetic micro-bearing based on 3D solenoidal micro-coils for advanced powerMEMS components, in: Proc. of PowerMEMS 2009, 2009, pp. 87–90.
- [37] Z. Lu, F. Jia, J. Korvink, U. Wallrabe, V. Badilita, Design optimization of an electromagnetic microlevitation system based on copper wirebonded coils, in: 2012 Power MEMS, Atlanta, GA, USA, 2012, pp. 363 – 366.

- [38] R. Krechetnikov, J. E. Marsden, On destabilizing effects of two fundamental non-conservative forces, *Physica D: Nonlinear Phenomena* 214 (1) (2006) 25–32.
- [39] A. Seyranian, W. Kliem, Metelitsyn’s inequality and stability criteria in mechanical problems, in: *Physics and Control, 2003. Proceedings. 2003 International Conference, Vol. 4, IEEE, 2003*, pp. 1096–1101.
- [40] E. B. Rosa, The self and mutual inductances of linear conductors, US Department of Commerce and Labor, Bureau of Standards, 1908.
- [41] F. Grover, Inductance calculations: working formulas and tables, Chicago: Dover publications, 2004.

Appendix A. Theorems

Three theorems with proofs are provided below, which establish the general stability issues of a micromachined inductive contactless suspension.

Theorem 1 (Unstable levitation I). *If a micromachined inductive suspension is subjected to only electromagnetic forces defined by (23) (without dissipation forces, so that $\mathbf{B} = 0$), then stable levitation in this suspension is impossible.*

Proof. According to the statement of the theorem, model (31) is rewritten as

$$\mathbf{A}\ddot{\mathbf{q}} + (\mathbf{R} + j\mathbf{P})\dot{\mathbf{q}} = 0. \quad (\text{A.1})$$

Let us consider two cases. The first case is when matrix \mathbf{R} is negative definite ($\mathbf{R} < 0$), and the second case is when matrix \mathbf{R} is positive definite ($\mathbf{R} > 0$).

The case of $\mathbf{R} < 0$ is the trivial one, since system (A.1) becomes unstable. Due to the fact that adding the positional forces to such a system cannot provide stable levitation [30, page 203, Theorem 6.13]. For $\mathbf{R} > 0$, system (A.1) can be transformed. Introducing a new complex vector $\bar{\mathbf{u}}$ such that

$$\bar{\mathbf{q}} = \Lambda \bar{\mathbf{u}}, \quad (\text{A.2})$$

where Λ is the orthogonal matrix of transformation, matrices \mathbf{A} and \mathbf{R} can be represented as

$$\Lambda^T \mathbf{A} \Lambda = \mathbf{I}, \quad \Lambda^T \mathbf{R} \Lambda = \mathbf{R}_0, \quad (\text{A.3})$$

where $\mathbf{R}_0 = \text{diag}(r_1, \dots, r_6)$ and \mathbf{I} is the identity matrix. Accounting for (A.2) and (A.3), model (A.1) becomes

$$\mathbf{I} \ddot{\mathbf{u}} + (\mathbf{R}_0 + j\hat{\mathbf{P}}) \bar{\mathbf{u}} = 0, \quad (\text{A.4})$$

where $\hat{\mathbf{P}} = \Lambda^T \mathbf{P} \Lambda$. Eq. (A.4) can be rewritten in real values as

$$\left(\begin{array}{c|c} \mathbf{I} & 0 \\ \hline 0 & \mathbf{I} \end{array} \right) \begin{pmatrix} \ddot{\mathbf{u}} \\ \ddot{\mathbf{u}}^* \end{pmatrix} + \left(\begin{array}{c|c} \mathbf{R}_0 & -\hat{\mathbf{P}} \\ \hline \hat{\mathbf{P}} & \mathbf{R}_0 \end{array} \right) \begin{pmatrix} \mathbf{u} \\ \mathbf{u}^* \end{pmatrix} = 0, \quad (\text{A.5})$$

for which the characteristic equation is

$$\det \left(\begin{array}{c|c} \mathbf{I}\lambda^2 + \mathbf{R}_0 & -\hat{\mathbf{P}} \\ \hline \hat{\mathbf{P}} & \mathbf{I}\lambda^2 + \mathbf{R}_0 \end{array} \right) = 0, \quad (\text{A.6})$$

or

$$\det \left((\mathbf{I}\lambda^2 + \mathbf{R}_0)^2 + \hat{\mathbf{P}}^2 \right) = 0. \quad (\text{A.7})$$

Due to the fact that matrix $\hat{\mathbf{P}}^2 > 0$ is positive definite, the following characteristic equation $\det (\tilde{\lambda}^2 + \hat{\mathbf{P}}^2) = 0$ has twelve imaginary roots, $\tilde{\lambda}_i = \pm ja_i$, $a_i > 0$, $i = (1, \dots, 6)$. Hence, accounting for $\tilde{\lambda}_i = \lambda^2 + r_i$, where $r_i > 0$, $i = (1, \dots, 6)$, the roots of (A.7) become

$$\begin{aligned} \lambda_i &= \pm j\sqrt{(r_i - ja_i)}, \quad i = (1, \dots, 6), \\ \lambda_j &= \pm j\sqrt{(r_j + ja_j)}, \quad j = (7, \dots, 12), \end{aligned} \quad (\text{A.8})$$

Finally, we have

$$\begin{aligned} \lambda_i &= \pm \sqrt{\frac{\sqrt{r_i^2 + a_i^2} - r_i}{2}} \pm j\sqrt{\frac{\sqrt{r_i^2 + a_i^2} + r_i}{2}}, \quad i = (1, \dots, 6) \\ \lambda_j &= \mp \sqrt{\frac{\sqrt{r_j^2 + a_j^2} - r_j}{2}} \pm j\sqrt{\frac{\sqrt{r_j^2 + a_j^2} + r_j}{2}}, \quad j = (7, \dots, 12) \end{aligned} \quad (\text{A.9})$$

From (A.9), it is seen that the real part of the roots have positive values. This fact proves the theorem.

Corollary 1.1. *If a micromachined inductive suspension is subjected to only*

electromagnetic forces, and the potential part of the electromagnetic forces is absent ($\mathbf{R} = 0$), then stable levitation in the suspension is impossible.

This fact follows directly from (A.9). Substituting $r_i = 0$ into (A.9), the roots still have a positive real part. Also, the corollary agrees with theorem [30, page 197, Theorem 6.10] about the equilibrium of a system subjected only to positional forces.

Theorem 2 (Unstable levitation II). *If a micromachined inductive suspension is subjected to electromagnetic forces having only positional $\mathbf{P} \neq 0$ ($\mathbf{R} = 0$) and dissipative forces ($\mathbf{B} > 0$), then stable levitation is impossible.*

Proof. We consider the following equation

$$\mathbf{A}\ddot{\mathbf{q}} + \mathbf{B}\dot{\mathbf{q}} + j\mathbf{R}\bar{\mathbf{q}} = 0. \quad (\text{A.10})$$

As it was done above, the complex vector $\bar{\mathbf{u}}$ given in (A.2) is used, hence matrices \mathbf{A} and \mathbf{B} can be represented as:

$$\Lambda^T \mathbf{A} \Lambda = \mathbf{I}, \quad \Lambda^T \mathbf{B} \Lambda = \mathbf{B}_0, \quad (\text{A.11})$$

where $\mathbf{B}_0 = \text{diag}(\hat{\mu}_1, \dots, \hat{\mu}_6)$. Taking later equations into account, Eq. (A.10) is rewritten as

$$\mathbf{I}\ddot{\mathbf{u}} + \mathbf{B}_0\dot{\mathbf{u}} + j\hat{\mathbf{P}}\bar{\mathbf{u}} = 0, \quad (\text{A.12})$$

where $\hat{\mathbf{P}} = \Lambda^T \mathbf{P} \Lambda$. Eq. (A.12) can be rewritten in real values as

$$\left(\begin{array}{c|c} \mathbf{I} & 0 \\ \hline 0 & \mathbf{I} \end{array} \right) \begin{pmatrix} \ddot{\mathbf{u}} \\ \ddot{\mathbf{u}}^* \end{pmatrix} + \left(\begin{array}{c|c} \mathbf{B}_0 & 0 \\ \hline 0 & \mathbf{B}_0 \end{array} \right) \begin{pmatrix} \dot{\mathbf{u}} \\ \dot{\mathbf{u}}^* \end{pmatrix} + \left(\begin{array}{c|c} 0 & -\hat{\mathbf{P}} \\ \hline \hat{\mathbf{P}} & 0 \end{array} \right) \begin{pmatrix} \mathbf{u} \\ \mathbf{u}^* \end{pmatrix} = 0. \quad (\text{A.13})$$

The characteristic equation is:

$$\det \left(\begin{array}{c|c} \mathbf{I}\lambda^2 + \mathbf{B}_0\lambda & -\hat{\mathbf{P}} \\ \hline \hat{\mathbf{P}} & \mathbf{I}\lambda^2 + \mathbf{B}_0\lambda \end{array} \right) = 0, \quad (\text{A.14})$$

or

$$\det \left((\mathbf{I}\lambda^2 + \mathbf{B}_0\lambda)^2 + \hat{\mathbf{P}}^2 \right) = 0. \quad (\text{A.15})$$

Using the same reasoning as for Theorem 1, the roots are:

$$\begin{aligned}\lambda_i &= \frac{-\hat{\mu}_i + \sqrt{\hat{\mu}_i^2 \mp j4a_i}}{2}, \quad i = (1, \dots, 6) \\ \lambda_j &= \frac{-\hat{\mu}_i - \sqrt{\hat{\mu}_i^2 \mp j4a_i}}{2}, \quad j = (7, \dots, 12)\end{aligned}\tag{A.16}$$

Here we need to prove that the real part of $\Re(\lambda_i) > 0$ is positive. Accounting for

$$\sqrt{\hat{\mu}_i^2 \mp j4a_i} = \sqrt{\frac{\sqrt{\hat{\mu}_i^4 + 16a_i^2} + \hat{\mu}_i^2}{2}} \mp j\sqrt{\frac{\sqrt{\hat{\mu}_i^4 + 16a_i^2} - \hat{\mu}_i^2}{2}},\tag{A.17}$$

the real part of λ_i is

$$\Re(\lambda_i) = \frac{1}{2} \left(-\hat{\mu}_i + \sqrt{\frac{\sqrt{\hat{\mu}_i^4 + 16a_i^2} + \hat{\mu}_i^2}{2}} \right).\tag{A.18}$$

We can write

$$-\hat{\mu}_i + \sqrt{\frac{\sqrt{\hat{\mu}_i^4 + 16a_i^2} + \hat{\mu}_i^2}{2}} > 0.\tag{A.19}$$

Inequality (A.19) is rewritten as

$$\sqrt{\hat{\mu}_i^4 + 16a_i^2} > \hat{\mu}_i^2,\tag{A.20}$$

which yields

$$16a_i^2 > 0.\tag{A.21}$$

This fact shows that the real part of λ_i is positive. Hence the theorem is proved.

It is important to note that Theorem 2 corresponds to Theorem [30, page 198, Theorem 6.11], which claims that the equilibrium of a system subjected to arbitrary nonconservative positional forces and linear dissipative forces is always unstable.

Theorem 3 (Asymptotically stable levitation). *By adding dissipative forces ($\mathbf{B} > 0$) to a micromachined inductive suspension subjected to electromagnetic forces defined by (23) and having a positive definite matrix of potential forces ($\mathbf{R} > 0$), the suspension can be asymptotically stable.*

Proof. In order to prove the theorem, Metelitsyn's inequality [31] is used [32,

page 32]. The necessary condition is that matrix \mathbf{A} , \mathbf{B} and \mathbf{R} should be positive definite. The condition follows from the statement of the theorem. According to [39, page 1099], a sufficient practical condition for asymptotically stable levitation for the present case becomes as follows

$$\mu_{\min} > p_{\max} \sqrt{a_{\max}/r_{\min}},$$

560 where μ_{\min} , and r_{\min} are the respective minimum values of \mathbf{B} and \mathbf{R} ; p_{\max} and a_{\max} are the respective maximum values of \mathbf{P} and \mathbf{A} . This fact proves that the real part of eigenvalues is negative when the inequality (36) holds true. Thus, the system is asymptotically stable.

Appendix B. Equation compilation for axially symmetric MIS

In order to find stiffness components for the model of 3D axially symmetric MIS, the structure of which has defined in Table 1, terms of Taylor series in (25) are calculated. Using the notation defined in Sec. 2 and Fig. 5(b), we can write for m_0^{kj} [7]:

$$\begin{aligned} m_0^{11} &= \sum_{\iota=0}^{N-1} \mu_0 \cdot r_s \left[\ln \frac{8r_s}{\sqrt{(h + \iota \cdot p)^2 + (d - c)^2}} - 1.92 \right]; \\ m_0^{22} &= \sum_{\iota=0}^{M-1} \mu_0 \cdot r_l \left[\ln \frac{8r_l}{h + \iota \cdot p} - 1.92 \right]; \\ m_0^{12} &= \sum_{\iota=0}^{M-1} \mu_0 \cdot (r_l + d) \left[\ln \frac{8(r_l + d)}{\sqrt{(h + \iota \cdot p)^2 + d^2}} - 1.92 \right]; \\ m_0^{21} &= \sum_{\iota=0}^{N-1} \mu_0 \cdot r_s \left[\ln \frac{8r_s}{\sqrt{(h + \iota \cdot p)^2 + c^2}} - 1.92 \right], \end{aligned} \tag{B.1}$$

where $\mu_0 = 4\pi \times 10^{-7}$ H/m is the magnetic permeability of vacuum, p is the winding pitch of the coils, $c = r_s - r_l$, N and M are numbers of winding for stabilization and levitation coils, respectively. According to [23] for the set of

terms m_l^{kj} we have:

$$\begin{aligned}
m_\nu^{11} &= - \sum_{\iota=0}^{N-1} \mu_0 \cdot r_s \frac{h + \iota \cdot p}{(h + \iota \cdot p)^2 + (c - d)^2}; \\
m_\nu^{22} &= - \sum_{\iota=0}^{M-1} \mu_0 \cdot r_l \frac{1}{h + \iota \cdot p}; \\
m_\nu^{12} &= - \sum_{\iota=0}^{M-1} \mu_0 \cdot (r_l + d) \frac{h + \iota \cdot p}{(h + \iota \cdot p)^2 + d^2}; \\
m_\nu^{21} &= - \sum_{\iota=0}^{N-1} \mu_0 \cdot r_s \frac{h + \iota \cdot p}{(h + \iota \cdot p)^2 + c^2}; \\
m_l^{11} &= m_l^{22} = m_l^{12} = m_l^{21} = 0; \\
m_\theta^{11} &= m_\theta^{22} = m_\theta^{12} = m_\theta^{21} = 0.
\end{aligned} \tag{B.2}$$

Terms of the second derivatives, m_{ll}^{kj} , are defined as follows. For $m_{\nu\nu}^{kj}$, we have:

$$\begin{aligned}
m_{\nu\nu}^{11} &= \sum_{\iota=0}^{N-1} \mu_0 \cdot r_s \frac{(h + \iota \cdot p)^2 - (c - d)^2}{[(h + \iota \cdot p)^2 + (c - d)^2]^2}; \\
m_{\nu\nu}^{22} &= \sum_{\iota=0}^{N-1} \mu_0 \cdot r_l \frac{1}{h + \iota \cdot p}; \\
m_{\nu\nu}^{12} &= \sum_{\iota=0}^{N-1} \mu_0 \cdot (r_l + d) \frac{(h + \iota \cdot p)^2 - d^2}{[(h + \iota \cdot p)^2 + d^2]^2}; \\
m_{\nu\nu}^{21} &= \sum_{\iota=0}^{N-1} \mu_0 \cdot r_s \frac{(h + \iota \cdot p)^2 - c^2}{[(h + \iota \cdot p)^2 + c^2]^2};
\end{aligned} \tag{B.3}$$

Taking into account the behaviour of the second circuit of eddy current shown in Fig. 5(b), for m_{ll}^{kj} we can write:

$$\begin{aligned}
m_{ll}^{11} &= \sum_{\iota=0}^{N-1} \mu_0 \cdot \frac{r_s (d - c)^2 r_s - (h + \iota \cdot p)^2 (r_s - 2c + 2d)}{2 (r_s - (c - d)) [(h + \iota \cdot p)^2 + (d - c)^2]^2}; \\
m_{ll}^{12} &= \sum_{\iota=0}^{N-1} \mu_0 \cdot \frac{r_l d^2 r_l - (h + \iota \cdot p)^2 (r_l + 2d)}{2 (r_l + d) [(h + \iota \cdot p)^2 + d^2]^2}; \\
m_{ll}^{21} &= m_{ll}^{22} = 0.
\end{aligned} \tag{B.4}$$

For $m_{\theta\theta}^{kj}$ we can write:

$$\begin{aligned}
m_{\theta\theta}^{11} &= (r_l + d)^2 \sum_{\iota=0}^{N-1} \mu_0 \cdot \frac{r_s}{2} \frac{(h + \iota \cdot p)^2 - (d - c)^2}{[(h + \iota \cdot p)^2 + (d - c)^2]^2}; \\
m_{\theta\theta}^{12} &= r_l^2 \sum_{\iota=0}^{N-1} \mu_0 \cdot \frac{r_s}{2} \frac{(h + \iota \cdot p)^2 - d^2}{[(h + \iota \cdot p)^2 + d^2]^2}; \\
m_{\theta\theta}^{21} &= (r_l + d)^2 \sum_{\iota=0}^{M-1} \mu_0 \cdot \frac{r_l}{2} \frac{(h + \iota \cdot p)^2 - d^2}{[(h + \iota \cdot p)^2 + d^2]^2}; \\
m_{\theta\theta}^{22} &= r_l^2 \sum_{\iota=0}^{M-1} \mu_0 \cdot \frac{r_l}{2} \frac{1}{(h + \iota \cdot p)^2}.
\end{aligned} \tag{B.5}$$

Terms of Taylor series for self and mutual inductances of eddy current circuits like g_0^{ks} , g_l^{ks} and g_{ll}^{ks} can be written as follows. Terms g_0^{ks} are:

$$\begin{aligned}
g_0^{11} &= \mu_0 \cdot (r_l + d) \left[\ln \frac{8(r_l + d)}{\chi} - 1.92 \right]; \\
g_0^{22} &= \mu_0 \cdot r_l \left[\ln \frac{8r_l}{\chi} - 1.92 \right]; \\
g_0^{12} &= g_0^{12} = \mu_0 \cdot (r_l + d) \left[\ln \frac{8(r_l + d)}{d} - 1.92 \right],
\end{aligned} \tag{B.6}$$

where χ is the characteristic length for eddy current circuit. Although,

$$g_l^{12} = g_\theta^{12} = g_\nu^{12} = 0 \tag{B.7}$$

and

$$g_{\theta\theta}^{12} = g_{\nu\nu}^{12} = 0, \tag{B.8}$$

however the second derivative with respect to generalized coordinate l is zero. Due to the behaviour of eddy current circuits shown in Fig. 5(b) it becomes as

$$g_{ll}^{12} = g_{ll}^{21} = \mu_0 \cdot \frac{r_l}{2} \frac{r_l}{(r_l + d)d^2}. \tag{B.9}$$

Using the equations above we can define determinants (15) and (19) as follows.

Determinants Δ_0^{ks} are:

$$\begin{aligned}
\Delta_0^{11} &= \begin{vmatrix} m_0^{11} & m_0^{21} \\ g_0^{21} & g_0^{22} \end{vmatrix}; \quad \Delta_0^{12} = \begin{vmatrix} m_0^{12} & m_0^{22} \\ g_0^{21} & g_0^{22} \end{vmatrix}; \\
\Delta_0^{21} &= \begin{vmatrix} g_0^{11} & g_0^{12} \\ m_0^{11} & m_0^{21} \end{vmatrix}; \quad \Delta_0^{22} = \begin{vmatrix} g_0^{11} & g_0^{12} \\ m_0^{12} & m_0^{22} \end{vmatrix}.
\end{aligned} \tag{B.10}$$

Determinant Δ_0 is

$$\Delta_0 = \begin{vmatrix} g_0^{11} & g_0^{12} \\ g_0^{21} & g_0^{22} \end{vmatrix}. \quad (\text{B.11})$$

Accounting for (B.2) and (B.7), Δ_l^{ks} are:

$$\begin{aligned} \Delta_\nu^{11} &= \begin{vmatrix} m_\nu^{11} & m_\nu^{21} \\ g_0^{21} & g_0^{22} \end{vmatrix}; \quad \Delta_\nu^{12} = \begin{vmatrix} m_\nu^{12} & m_\nu^{22} \\ g_0^{21} & g_0^{22} \end{vmatrix}; \\ \Delta_\nu^{21} &= \begin{vmatrix} g_0^{11} & g_0^{12} \\ m_\nu^{11} & m_\nu^{21} \end{vmatrix}; \quad \Delta_\nu^{22} = \begin{vmatrix} g_0^{11} & g_0^{12} \\ m_\nu^{12} & m_\nu^{22} \end{vmatrix}, \end{aligned} \quad (\text{B.12})$$

and others Δ_l^{ks} and Δ_θ^{ks} are zero. The first derivative of (B.11) is also zero. Accounting for (B.3), (B.4), (B.5) and (B.9), the second derivatives of the determinants are written as follows. With respect to ν :

$$\begin{aligned} \Delta_{\nu\nu}^{11} &= \begin{vmatrix} m_{\nu\nu}^{11} & m_{\nu\nu}^{21} \\ g_0^{21} & g_0^{22} \end{vmatrix}; \quad \Delta_{\nu\nu}^{12} = \begin{vmatrix} m_{\nu\nu}^{12} & m_{\nu\nu}^{22} \\ g_0^{21} & g_0^{22} \end{vmatrix}; \\ \Delta_{\nu\nu}^{21} &= \begin{vmatrix} g_0^{11} & g_0^{12} \\ m_{\nu\nu}^{11} & m_{\nu\nu}^{21} \end{vmatrix}; \quad \Delta_{\nu\nu}^{22} = \begin{vmatrix} g_0^{11} & g_0^{12} \\ m_{\nu\nu}^{12} & m_{\nu\nu}^{22} \end{vmatrix}; \end{aligned} \quad (\text{B.13})$$

with respect to θ :

$$\begin{aligned} \Delta_{\theta\theta}^{11} &= \begin{vmatrix} m_{\theta\theta}^{11} & m_{\theta\theta}^{21} \\ g_0^{21} & g_0^{22} \end{vmatrix}; \quad \Delta_{\theta\theta}^{12} = \begin{vmatrix} m_{\theta\theta}^{12} & m_{\theta\theta}^{22} \\ g_0^{21} & g_0^{22} \end{vmatrix}; \\ \Delta_{\theta\theta}^{21} &= \begin{vmatrix} g_0^{11} & g_0^{12} \\ m_{\theta\theta}^{11} & m_{\theta\theta}^{21} \end{vmatrix}; \quad \Delta_{\theta\theta}^{22} = \begin{vmatrix} g_0^{11} & g_0^{12} \\ m_{\theta\theta}^{12} & m_{\theta\theta}^{22} \end{vmatrix}; \end{aligned} \quad (\text{B.14})$$

and with respect to l we have

$$\begin{aligned}
\Delta_{ll}^{11} &= \begin{vmatrix} m_{ll}^{11} & 0 \\ g_0^{21} & g_0^{22} \end{vmatrix} + \begin{vmatrix} m_0^{11} & m_0^{21} \\ g_{ll}^{21} & 0 \end{vmatrix}; \\
\Delta_{ll}^{12} &= \begin{vmatrix} m_{ll}^{12} & 0 \\ g_0^{21} & g_0^{22} \end{vmatrix} + \begin{vmatrix} m_0^{12} & m_0^{22} \\ g_{ll}^{21} & 0 \end{vmatrix}; \\
\Delta_{ll}^{21} &= \begin{vmatrix} 0 & g_{ll}^{12} \\ m_0^{11} & m_0^{21} \end{vmatrix} + \begin{vmatrix} g_0^{11} & g_0^{12} \\ m_{ll}^{11} & 0 \end{vmatrix}; \\
\Delta_{ll}^{22} &= \begin{vmatrix} 0 & g_{ll}^{12} \\ m_0^{12} & m_0^{22} \end{vmatrix} + \begin{vmatrix} g_0^{11} & g_0^{12} \\ m_{ll}^{12} & 0 \end{vmatrix}.
\end{aligned} \tag{B.15}$$

For determinant (B.11) only the second derivative with respect to l exists and becomes as

$$\Delta_{ll} = \begin{vmatrix} 0 & g_{ll}^{12} \\ g_0^{21} & g_0^{22} \end{vmatrix} + \begin{vmatrix} g_0^{11} & g_0^{12} \\ g_{ll}^{21} & 0 \end{vmatrix}. \tag{B.16}$$

565 **Appendix C. Equation compilation for 3D linear transporter**

The scheme for the calculation of the stiffness and stability of the transporter is shown in Fig. 11(a). Using equations for self-inductances of a rectangle and straight wire having a square cross-section [40, pages 320 and 315], respectively, and mutual inductance of two parallel wires [40, page 306], terms g_0^{ks} of (25)

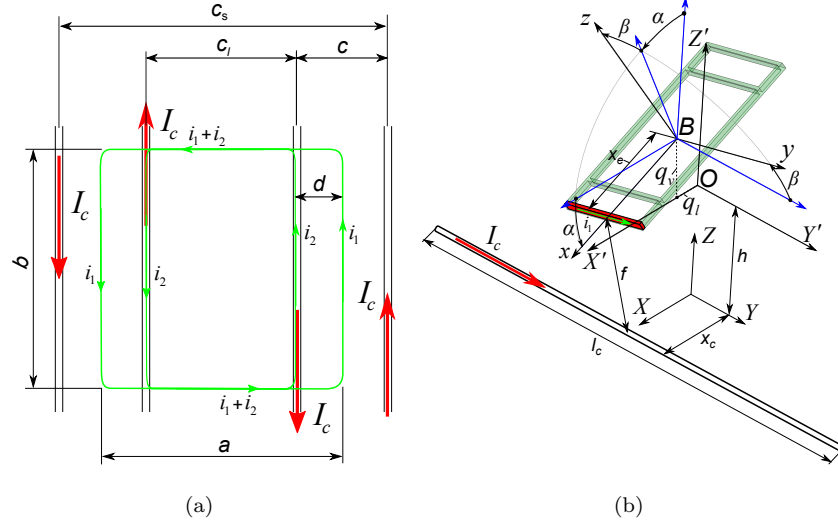


Figure C.11: Scheme of transporter for calculation.

can be defined as:

$$\begin{aligned}
 g_0^{11} &= \frac{\mu_0}{\pi} \cdot (c_l + 2d + b) \left[\ln \frac{2(c_l + 2d)b}{\chi} - \frac{(c_l + 2d) \ln(c_l + 2d + b) + b \ln(c_l + 2d + b)}{c_l + 2d + b} \right. \\
 &\quad \left. + \frac{\sqrt{(c_l + 2d)^2 + b^2}}{c_l + 2d + b} - \frac{1}{2} + 0.477 \frac{\chi}{c_l + 2d + b} \right]; \\
 g_0^{22} &= \frac{\mu_0}{\pi} \cdot (c_l + b) \left[\ln \frac{2c_l b}{\chi} - \frac{c_l \ln(c_l + b) + b \ln(c_l + b)}{c_l + b} + \frac{\sqrt{c_l^2 + b^2}}{c_l + b} - \frac{1}{2} + 0.477 \frac{\chi}{c_l + b} \right]; \\
 g_0^{12} = g_0^{21} &= \frac{\mu_0 c_l}{\pi} \left[\ln \frac{c_l}{\chi} + \frac{1}{2} \right] + \frac{\mu_0 b}{\pi} \left[\ln \frac{b + \sqrt{b^2 + d^2}}{d} - \frac{\sqrt{b^2 + d^2}}{b} + \frac{d}{b} \right] \\
 &\quad - \frac{\mu_0 b}{\pi} \left[\ln \frac{b + \sqrt{b^2 + (d + c_l)^2}}{d + c_l} - \frac{\sqrt{b^2 + (d + c_l)^2}}{b} + \frac{d + c_l}{b} \right],
 \end{aligned} \tag{C.1}$$

where $d = (a - c_l)/2$. As it follows from the analysis of scheme shown in Fig. 11(a), the mutual inductances between the coils' wires and the levitated micro-object are reduced to the analysis of the mutual inductance of the system of the parallel wires. In order to compile the terms of (25) let us define the mutual inductance between coil's straight wire and an element of eddy current circuit as it is shown in Fig. 11(b). The element of eddy current circuit is highlighted in red. Using equation of mutual inductance of two parallel wires

[40, page 306] having the same length, l_c , the following auxiliary function can be defined as

$$M_a(l_c, f(x_e, x_c)) = \frac{\mu_0 l_c}{\pi} \left[\ln \frac{1 + \sqrt{1 + \xi^2}}{\xi} - \sqrt{1 + \xi^2} + \xi \right], \quad (\text{C.2})$$

where $\xi = f/l_c$ is the dimensionless parameter, l_c is the length of the coil wire, f is the distance between two wires, which can be calculated as

$$f(x_e, x_c) = \sqrt{(h + q_v - x_e \sin \alpha)^2 + (x_c - x_e \cos \alpha + q_l)^2}, \quad (\text{C.3})$$

where x_c is the coordinate of location of the coil wire along the X -axis and x_e is the coordinate of location of the element of eddy current circuit along the X' -axis (equilibrium state) as shown in Fig. 11(b). Assuming that the displacements are small and using auxiliary function (C.2), the mutual inductance between element of the eddy current circuit and coil's wire as shown in Fig. 11(b) can be written as [41, page 45]:

$$M(x_e, x_c) = (M_a((l_c + b \cos \beta)/2, f(x_e, x_c)) - M_a((l_c - b \cos \beta)/2, f(x_e, x_c))). \quad (\text{C.4})$$

Noting that the latter equation is derived for the case when the geometrical centers of the coil wire and element of eddy current circuit are aligned. In order to take into account the number of windings, Eq. (C.4) can be modified as follows

$$M_\iota(x_e, x_c) = (M_a((l_c + b \cos \beta)/2, f_\iota(x_e, x_c)) - M_a((l_c - b \cos \beta)/2, f_\iota(x_e, x_c))). \quad (\text{C.5})$$

where

$$f_\iota(x_e, x_c) = \sqrt{(h + p \cdot \iota + q_v - x_e \sin \alpha)^2 + (x_c - x_e \cos \alpha + q_l)^2}. \quad (\text{C.6})$$

Hence, considering pairwise wires of coils and accounting for (C.5) terms m_0^{kj} are

$$\begin{aligned}
m_0^{11} &= 2 \sum_{\substack{\iota=0 \\ M-1}}^{N-1} [M_\iota(c_l/2 + d, c_s/2) - M_\iota(-c_l/2 - d, c_s/2)]; \\
m_0^{22} &= 2 \sum_{\substack{\iota=0 \\ M-1}}^{N-1} [M_\iota(c_l/2, c_l/2) - M_\iota(-c_l/2, c_l/2)]; \\
m_0^{12} &= 2 \sum_{\substack{\iota=0 \\ N-1}}^{M-1} [M_\iota(c_l/2 + d, c_l/2) - M_\iota(-c_l/2 - d, c_l/2)]; \\
m_0^{21} &= 2 \sum_{\iota=0}^{N-1} [M_\iota(c_l/2, c_s/2) - M_\iota(-c_l/2, c_s/2)].
\end{aligned} \tag{C.7}$$

For deriving derivatives of (C.5) with respect generalized coordinates q_v , q_l and α , a general rule can be used such as

$$\begin{aligned}
\frac{\partial M_a}{\partial q} &= \frac{\partial M_a}{\partial \xi} \frac{\partial \xi}{\partial q}; \\
\frac{\partial^2 M_a}{\partial q^2} &= \frac{\partial^2 M_a}{\partial \xi^2} \left(\frac{\partial \xi}{\partial q} \right)^2 + \frac{\partial M_a}{\partial \xi} \frac{\partial^2 \xi}{\partial q^2}.
\end{aligned} \tag{C.8}$$

The ξ - derivatives of M_a are

$$\begin{aligned}
\frac{\partial M_a}{\partial \xi} &= \frac{\mu_0 l_c}{\pi} \left[1 - \frac{1}{\xi} - \frac{\xi}{1 + \sqrt{1 + \xi^2}} \right]; \\
\frac{\partial^2 M_a}{\partial \xi^2} &= \frac{\mu_0 l_c}{\pi} \left[\frac{1}{\xi^2} - \frac{1}{(1 + \sqrt{1 + \xi^2})\sqrt{1 + \xi^2}} \right].
\end{aligned} \tag{C.9}$$

The derivatives of ξ with respect to q_v at the equilibrium point:

$$\begin{aligned}
\frac{\partial \xi}{\partial q_v} &= \frac{1}{l_c} \frac{h}{\sqrt{h^2 + (x_c - x_e)^2}}; \\
\frac{\partial^2 \xi}{\partial q_v^2} &= \frac{1}{l_c} \frac{(x_c - x_e)^2}{\sqrt[3]{h^2 + (x_c - x_e)^2}}.
\end{aligned} \tag{C.10}$$

The derivatives of ξ with respect to q_l at the equilibrium point:

$$\begin{aligned}
\frac{\partial \xi}{\partial q_l} &= \frac{1}{l_c} \frac{x_c - x_e}{\sqrt{h^2 + (x_c - x_e)^2}}; \\
\frac{\partial^2 \xi}{\partial q_l^2} &= \frac{1}{l_c} \frac{h^2}{\sqrt[3]{h^2 + (x_c - x_e)^2}}.
\end{aligned} \tag{C.11}$$

The derivatives of ξ with respect to α at the equilibrium point:

$$\begin{aligned}
\frac{\partial \xi}{\partial \alpha} &= \frac{1}{l_c} \frac{x_e h}{\sqrt{h^2 + (x_c - x_e)^2}}; \\
\frac{\partial^2 \xi}{\partial \alpha^2} &= \frac{1}{l_c} \frac{x_e^2 (x_c - x_e)^2}{\sqrt[3]{h^2 + (x_c - x_e)^2}}.
\end{aligned} \tag{C.12}$$

The cross-derivatives of ξ are

$$\begin{aligned}\frac{\partial^2 \xi}{\partial q_v \partial \alpha} &= \frac{1}{l_c} \frac{x_e(x_c - x_e)^2}{\sqrt[3]{h^2 + (x_c - x_e)^2}}; \\ \frac{\partial^2 \xi}{\partial q_l \partial \alpha} &= -\frac{1}{l_c} \frac{x_e h(x_c - x_e)}{\sqrt[3]{h^2 + (x_c - x_e)^2}}; \\ \frac{\partial^2 \xi}{\partial q_l \partial q_v} &= -\frac{1}{l_c} \frac{h(x_c - x_e)}{\sqrt[3]{h^2 + (x_c - x_e)^2}}.\end{aligned}\tag{C.13}$$

For generalized coordinates q_v , q_l and α the derivative of $M_l(x_e, x_c)$ with respect to these coordinates has the following general form:

$$\frac{\partial M_{(x_e, x_c), l}}{\partial q} = \frac{\partial M_a}{\partial \xi'_l} \frac{\partial \xi'_l}{\partial q} - \frac{\partial M_a}{\partial \xi''_l} \frac{\partial \xi''_l}{\partial q},\tag{C.14}$$

where $\xi'_l = 2f_l(x_e, x_c)/(l_c + b)$ and $\xi''_l = 2f_l(x_e, x_c)/(l_c - b)$. Let us consider separately derivative of M_l with respect to β . Starting with the estimation of derivative of ξ'_l with respect to β at the equilibrium point we have

$$\begin{aligned}\frac{\partial \xi'_l}{\partial \beta} &= 0; \\ \frac{\partial^2 \xi'_l}{\partial \beta^2} &= 2f_l(x_e, x_c) \frac{b}{(l_c + b)^2}.\end{aligned}\tag{C.15}$$

Accounting for the later equations, the first and the second β - derivative of $M_a((l_c + b \cos \beta)/2, f_l(x_e, x_c))$ for equilibrium point can be written as

$$\begin{aligned}\frac{\partial M_a}{\partial \beta} &= 0; \\ \frac{\partial^2 M_a}{\partial \beta^2} &= \frac{\partial M_a}{\partial \xi'_l} \frac{\partial^2 \xi'_l}{\partial \beta^2} - \frac{\mu_0 b}{2\pi} \left[\ln \frac{1 + \sqrt{1 + \xi'^2_l}}{\xi'_l} - \sqrt{1 + \xi'^2_l} + \xi'_l \right].\end{aligned}\tag{C.16}$$

For terms m_l^{kj} , we can write

$$\begin{aligned}
m_v^{11} &= 2 \sum_{\iota=0}^{N-1} \left[\frac{\partial M_{(c_l/2+d, c_s/2), \iota}}{\partial q} - \frac{\partial M_{(-c_l/2-d, c_s/2), \iota}}{\partial q} \right]; \\
m_v^{22} &= 2 \sum_{\iota=0}^{M-1} \left[\frac{\partial M_{(c_l/2, c_l/2), \iota}}{\partial q} - \frac{\partial M_{(-c_l/2, c_l/2), \iota}}{\partial q} \right]; \\
m_v^{12} &= 2 \sum_{\iota=0}^{M-1} \left[\frac{\partial M_{(c_l/2+d, c_l/2), \iota}}{\partial q} - \frac{\partial M_{(-c_l/2-d, c_l/2), \iota}}{\partial q} \right]; \\
m_v^{21} &= 2 \sum_{\iota=0}^{N-1} \left[\frac{\partial M_{(c_l/2, c_s/2), \iota}}{\partial q} - \frac{\partial M_{(-c_l/2, c_s/2), \iota}}{\partial q} \right]; \\
m_l^{11} &= m_l^{22} = m_l^{12} = m_l^{21} = 0; \\
m_\alpha^{11} &= m_\alpha^{22} = m_\alpha^{12} = m_\alpha^{21} = 0; \\
m_\beta^{11} &= m_\beta^{22} = m_\beta^{12} = m_\beta^{21} = 0.
\end{aligned} \tag{C.17}$$

Terms m_{ll}^{kj} can be written as follows. For generalized coordinate, q_l , we have

$$\begin{aligned}
m_{ll}^{11} &= 2 \sum_{\iota=0}^{N-1} \left[\frac{\partial^2 M_{(c_l/2+d, c_s/2), \iota}}{\partial q_l^2} - \frac{\partial^2 M_{(-c_l/2-d, c_s/2), \iota}}{\partial q_l^2} \right]; \\
m_{ll}^{12} &= 2 \sum_{\iota=0}^{M-1} \left[\frac{\partial^2 M_{(c_l/2+d, c_l/2), \iota}}{\partial q_l^2} - \frac{\partial^2 M_{(-c_l/2-d, c_l/2), \iota}}{\partial q_l^2} \right]; \\
m_{ll}^{22} &= 0; m_{ll}^{21} = 0.
\end{aligned} \tag{C.18}$$

For other generalized coordinates q_v, α and β , the second derivatives can be found by using the general rule given below

$$\begin{aligned}
m_{qq}^{11} &= 2 \sum_{\iota=0}^{N-1} \left[\frac{\partial^2 M_{(c_l/2+d, c_s/2), \iota}}{\partial q^2} - \frac{\partial^2 M_{(-c_l/2-d, c_s/2), \iota}}{\partial q^2} \right]; \\
m_{qq}^{12} &= 2 \sum_{\iota=0}^{M-1} \left[\frac{\partial^2 M_{(c_l/2+d, c_l/2), \iota}}{\partial q^2} - \frac{\partial^2 M_{(-c_l/2-d, c_l/2), \iota}}{\partial q^2} \right]; \\
m_{qq}^{22} &= 2 \sum_{\iota=0}^{M-1} \left[\frac{\partial^2 M_{(c_l/2, c_l/2), \iota}}{\partial q^2} - \frac{\partial^2 M_{(-c_l/2, c_l/2), \iota}}{\partial q^2} \right]; \\
m_{qq}^{21} &= 2 \sum_{\iota=0}^{M-1} \left[\frac{\partial^2 M_{(c_l/2, c_s/2), \iota}}{\partial q^2} - \frac{\partial^2 M_{(-c_l/2, c_s/2), \iota}}{\partial q^2} \right].
\end{aligned} \tag{C.19}$$

Similar to axially symmetric design Appendix B, terms g_l^{ks} are zero for all generalized coordinates. Terms g_{ll}^{ks} are zero only for coordinates q_v, α and β , while accounting for (C.2) the second derivative with respect to q_l can be written

as

$$g_{ll}^{12} = g_{ll}^{21} = 2 [M_a(b, f(c_l/2 + d, c_l/2)) - M_a(b, f(c_l/2 + d, -c_l/2))] . \quad (\text{C.20})$$

Hence, the determinants Δ^{ks} , Δ_0^{ks} , Δ_v^{ks} , Δ_{vv}^{ks} and Δ_{ll}^{ks} can be defined similar to (B.11), (B.10), (B.12), (B.13) and (B.16), respectively, whereas both $\Delta_{\alpha\alpha}^{ks}$ and $\Delta_{\beta\beta}^{ks}$ are similar to (B.14).